DFT study on Mo-stabilized passive films: Hydroxylation effects on chromium and iron oxide surfaces

Xian Huang, Dominique Costa, Boubakar Diawara, Vincent Maurice, Philippe Marcus

Author preprint published in *Corrosion Science*
https://doi.org/10.1016/j.corsci.2024.112105

DFT study on Mo-stabilized passive films: Hydroxylation effects on chromium and iron oxide surfaces

Xian Huang, Dominique Costa*, Boubakar Diawara, Vincent Maurice, Philippe Marcus*

PSL Research University, CNRS - Chimie ParisTech, Institut de Recherche de Chimie Paris, 11 rue Pierre et Marie Curie, 75005 Paris, France.

* Corresponding authors: dominique.costa@chimieparistech.psl.eu (D. Costa) and philippe.marcus@chimieparistech.psl.eu (P. Marcus).

Abstract

Hydrous Cr_2O_3 and Fe_2O_3 surfaces without and with substitutional molybdenum were simulated by DFT modelling to investigate at the atomic scale the role of Mo in improving the corrosion resistance of passive films on stainless steels. The surface structures most energetically favoured were determined in the conditions of interest. For surfaces with a high degree of hydroxylation, the preferential location of substitutional Mo is just under the hydroxyl groups, in agreement with the experimental observations. The substitution by Mo is exothermic and Mo preferentially substitutes in Fe- than in Cr-rich zone of the inner barrier layer of passive films.

Keywords

(A) stainless steel, (A) Cr_2O_3 and Fe_2O_3, (B) DFT, (C) passive films, (C) Mo effects, (C) hydrous surfaces

1. Introduction

Passive films formed on the surface provide excellent corrosion resistance for stainless steels [1] and other Cr-containing stainless alloys [2,3]. These nanometre-thick films are commonly composed of an inner Cr-rich oxide layer and an outer layer containing oxides and hydroxides [1–3]. On stainless steel, some weak sites of corrosion protection, where Fe is locally enriched instead of Cr, have been shown to form in the inner layer at the nanometre scale owing to the failure of the local supply of Cr upon initial growth of the oxide film [4,5]. On Mo-bearing multi-principal element alloys (Cr-Fe-Co-Ni-Mo) of higher Mo content than stainless steel,

which show enhanced passivity in concentrated Cl-containing environments [6,7], Mo(IV) and more positive Mo(IV+δ) species were observed concentrated at the interface between inner and outer layers and in the inner layer, respectively, suggesting that the Fe-rich weak sites of corrosion protection could be cured by the presence of Mo. This hypothesis was reinforced by density functional theory (DFT) modelling of the substitution of a metal cation by Mo, and its effects on charge localization and vacancy formation performed on (0001)-oriented chromia and hematite surfaces [8]. Substitution by Mo was found always exothermic and more favoured energetically on Fe_2O_3 than on Cr_2O_3 surfaces with substitutional Mo carrying more positive charge in the hematite than in the chromia defective matrix, suggesting that Mo may be preferentially more enriched as Mo(IV+δ) in the Fe-rich than in the Cr-rich oxide zones in passive films. The presence of substitutional Mo was found to disfavour O vacancies and favour metal cation vacancies, more significantly in Fe_2O_3 than in Cr_2O_3, indicating that the Cl penetration via O vacancies could be limited and that the replacement of Fe by Cr by local selective dissolution of the Fe-rich weak sites could be promoted. These data were comprehensively discussed to unravel the multiple effects that molybdenum might have at the nanometre and atomic scales to enhance the stability of passive films in chloride-containing environment [9]. In the present study, we further developed and completed the DFT approach by considering hydrated chromium and iron oxide surfaces, to model the presence of the outer hydroxide layer of the passive film and to understand in more details the stabilizing effects of Mo on the passivity of stainless steels and other alloys.

Chromia and hematite have the corundum structure in which the O atoms form a hexagonal close-packed lattice with 2/3 of the O octahedral sites occupied by Cr or Fe atoms, so the four-digit Miller index notation is used for oxide films. The (0001) surfaces of chromia and hematite are of interest here since the inner layers of the oxide films formed on many alloys with cubic crystal structures (body-centred cubic Cr(110) [10,11] and FeCr(110) [12] and face-centred cubic FeCrNi(100) [13]) are oriented to the [0001] direction according to experimental analyses. Anhydrous (0001) surfaces can be double-M-terminated ($-O_3-M_2$), single-M-terminated ($-O_3-M$) or O-terminated ($-M_2O_3$), with M for Cr or Fe atom. Experiments suggested single-M termination for the surfaces of chromia oxide films on Cr(110) [14–16] and bulk hematite [17], while the surface of hematite film epitaxially grown on Pt(111) was reported to be O-terminated [18]. Different theoretical surface phase diagrams have been calculated for chromia and hematite using the surface free energies obtained from DFT calculations [19–23].

Experimentally, hydrous (0001)-oriented surfaces of α-Cr_2O_3 grown on α-Al_2O_3 were characterized by temperature programmed desorption (TPD) after water exposure [24], finding that about two H_2O (1.2×10^{15} molecule.cm^{-2}) were adsorbed for each outermost Cr atom (4.8×10^{14} atom.cm^{-2} on ideal single-Cr-terminated surface). High resolution electron energy-loss spectroscopy (HREELS) and X-ray photoelectron spectroscopy (XPS) [24] suggested that for the two adsorbed H_2O, one was dissociated and the other was molecular, both with a surface coverage of about 4.6×10^{14} molecule.cm^{-2}. However, the surface structure beneath the water/hydroxyl monolayer was supposed to be single-Cr-terminated as on anhydrous surface, which might not be the case in ultrathin oxide film supported on a Cr-containing metal. In a

recent study with surface X-ray diffraction (SXRD) [25], it was reported that the (0001) surface of single crystalline bulk Cr_2O_3 had a termination near -Cr-$Cr_{0.74}$-$O_{1.11}$-$Cr_{0.26}$-$Cr_{0.10}$ in UHV condition with very low water exposure. At high water exposure near 100% humidity, each terminating Cr was found associated with an O atom from OH or H_2O, and the optimal surface structure that fitted the SXRD data was very complex (similar to -Cr-$Cr_{0.70}$-$O_{1.3}$-$Cr_{0.28}$-$Cr_{0.08}$ beneath the water/hydroxyl monolayer). Double-Cr terminated surfaces were considered here but the content of the terminating Cr atom seemed too small (0.08) to consider its existence. According to XPS analysis on Cr_2O_3 epitaxially grown on Cr(110) [26], the terminating OH groups (1.6×10^{15} atom.cm^{-2}) and the underneath Cr atoms (1.9×10^{15} atom.cm^{-2}) had very high coverages (note that the density is 1.5×10^{15} atom.cm^{-2} for O plane in the bulk) on surfaces after high water exposure. However, in a well-defined Cr_2O_3 matrix where Cr occupies 2/3 of the octahedral sites of O HCP lattice, the maximal Cr surface concentration cannot exceed that of O. Further, scanning tunnelling microscopy (STM) analysis on epitaxial Cr_2O_3 films [26] indicated that the surface was roughened after water exposure. On the passive films electrochemically formed on Cr(110) [11], STM observation suggested that the surface was stepped, terminated by a monolayer of hydroxyl or hydroxide groups.

On (0001)-oriented surfaces of monocrystalline α-Fe_2O_3, H_2O adsorbed dissociatively has been observed for water exposure above 10^3 L according to Ultraviolet Photoemission Spectroscopy (UPS) [27]. In a study using XPS, hydroxyl groups were also detected before molecular H_2O when increasing relative humidity starting from UHV conditions [28]. On the acid-etched surface of native hematite, STM observations and analysis show evidence of the coexistence of Fe- and (bare or protonated) O-terminations [29]. In another work, the characterization by Crystal Truncation Rod (CTR) on such kind of hydrous surface revealed a structure of -O_3-$Fe_{0.4}$-$O_{1.2}$ where O can be protonated [30]. Combining with DFT calculations, two kinds of hydroxylated surface structures were suggested: single-Fe termination with full dissociative adsorption (-$(OH)_3Fe(OH)_3$) and O-termination with full proton adsorption (-O_3-Fe_2-$(OH)_3$).

Theoretically, water adsorption on (0001)-oriented Cr_2O_3 was investigated by quantum chemical calculations on the single-Cr-terminated surface with the terminating Cr on different surface sites [31]. Dissociative adsorption on the terminating Cr at its bulk position was the most stable configuration for adsorbing one single H_2O molecule. Adsorption on the same surface structure had been studied by Costa *et al*. using DFT calculations [32,33]. The energies of molecular and dissociative adsorption were very close for adsorbing 1 H_2O per terminating Cr. Complementary *ab initio* molecular dynamic simulations at 300 K showed that proton could transfer easily between the water molecule and the outermost O atoms with a low activation energy of water dissociation (12 kJ.mol^{-1}). For 2 H_2O per terminating Cr, both adsorbed H_2O should be dissociated. In addition, the 3rd adsorbed H_2O was molecular. The phase diagram of different surfaces was computed based on the obtained DFT energies, suggesting that the surface with 3 H_2O per terminating Cr was favoured in air at room temperature. Water adsorption on single-M-terminating surfaces was also simulated by Souvi *et al.* for both Cr_2O_3 and Fe_2O_3 [21,22] but different results were obtained: the first H_2O molecule was adsorbed dissociatively while the second and the third was adsorbed without water dissociation. In the

same work, adsorption on a special O-terminated Cr_2O_3 surface ($-Cr_2O_{3/2}$) was also considered and the fully hydroxylated surface ($-Cr_2(OH)_3$) was found to be the most stable for water partial pressure lower than 3 bars at room temperature. The latter structure is equivalent to an O-terminated surface with full hydrogen adsorption or a double-Cr-terminated surface with full hydroxyl radical adsorption (or homolytic dissociative water adsorption). Such hydroxyl adsorption was also considered in the studies for hydrous Fe_2O_3 surfaces [34–37]. In a recent study using ab initio molecular dynamics to simulate Fe_2O_3 slab in liquid water under external electric field [38], it was found that H^+ ion from dissociative water adsorbed at an interface transferred in liquid water along the field direction to accumulate at another interface, suggesting the possibility of hydrogen or hydroxyl adsorption on surfaces during some electrochemical process.

On hydrous chromia and hematite surfaces with double-M termination under the OH monolayer ($-M_2(OH)_3$), Ng *et al.* [39] have investigated the oxygen reduction reaction on the oxide surfaces which played the role of cathodes for the anodic dissolution of metal in localized corrosion. It was reported that the activation energy, higher on the chromia than on the hematite surface, increased after substitution of Cr or Fe by Mo, suggesting that the substitutional Mo reinforced the corrosion resistance by slowing down the cathodic activity. To better understand the Mo effects on the reinforcement of corrosion resistance, more studies on hydrous surfaces are needed.

In the present work, we performed DFT+U calculations to investigate the Mo effects on (0001)-oriented surfaces of chromia (α-Cr_2O_3) and hematite (α-Fe_2O_3), hereafter denoted as Cr_2O_3 and Fe_2O_3, respectively. Anhydrous and hydrous surfaces without Mo were studied at first, followed by the investigation on the substitution by Mo on hydrous surfaces. The analysis of energies and charges provides atomistic insight into the properties of Mo-enhanced passive films formed on the surfaces of stainless steel and other Cr-containing alloys.

2. Method

As introduced above, passive oxide films formed on Cr-containing alloys [1–3] have a bilayer structure with an inner barrier layer markedly enriched in chromium oxide and an outer layer formed by oxides and hydroxides of chromium and other alloying elements. Figure 1(a) illustrates such a chemical duplex structure reported for the passive film formed on a Cr-Fe-Co-Ni-Mo multi-principal element alloy [9]. In our previous work [8], a simplified model considering anhydrous Cr_2O_3 surfaces, was used to investigate Mo effects. In the present work, hydroxyl groups were added on the surfaces to form hydrous surfaces. Figure 1(b) shows the model with hydroxyl groups of full coverage, resulting in a monolayer of hydroxide of chromium that can be used to simulate the duplex experimental structures. Fe_2O_3, which has the same corundum structure as Cr_2O_3, has also been investigated in order to compare with Cr_2O_3. To explain concisely the calculation details, we use Cr_2O_3 as an example and give the relevant details for Fe_2O_3 in supporting information (SI).

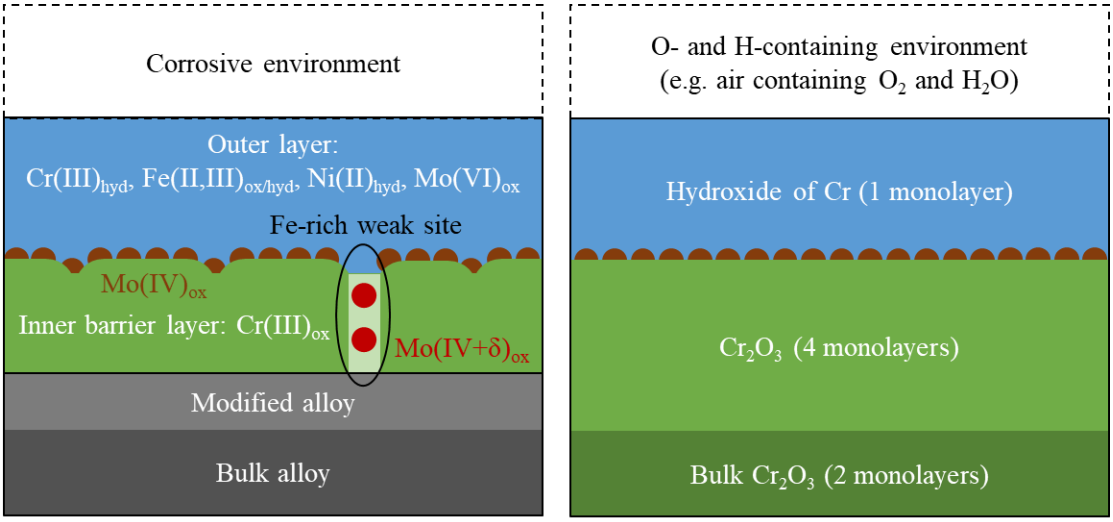

(a) model from the experiments (b) model in simulations

Figure 1. (a) Model of passive films formed on Cr-containing alloys proposed from experiments on Cr-Fe-Co-Ni-Mo multi-principal element alloys [9] and (b) model used in present simulations for Cr_2O_3.

Hexagonal unit cell (30 atoms) of bulk Cr_2O_3 with an atomic stacking …-Cr-O_3-Cr-… in [0001] direction was used as a starting point to generate slabs. Figure 2 shows the three slabs used in the present work. Vacuum with a thickness of at least 25 Å was inserted at equidistance of two consecutive Cr half-layers to generate a single-Cr-terminated (0001)-oriented symmetric slab which contained 6 -Cr-O_3-Cr- monolayers. Before surface relaxation, all atoms were in their bulk positions and the slab had symmetric unrelaxed single-Cr-terminated surfaces both at the top and bottom of the slab, allowing us to deduce the energy of the unrelaxed surface. During surface relaxation, 4 monolayers from the top of the slab were relaxed while 2 monolayers from the bottom were frozen. The numbers of relaxed and frozen monolayers, determined in our previous work [8], were large enough to avoid the influence of the bottom unrelaxed surface on the top surface. After relaxation, the slab became asymmetric with relaxed and unrelaxed single-Cr-terminated surfaces at the top and bottom, respectively (Figure 2(a)).

Single-Cr-terminated surfaces can transform to double-Cr-terminated surfaces (assembling two terminating Cr on one surface and releasing three O) and then to O-terminated surfaces (adsorbing three O). To construct double-Cr-terminated surfaces, one Cr atom was added initially in the bulk position both on the top and at the bottom of the single-Cr-terminated slab. Figure 2(b) shows the relaxed structure. For O-terminated surfaces, when three O atoms were added in the bulk positions both on the top and at the bottom of the double-Cr-terminated slab, the electronic cycle could not well converge for calculating the energy of the unrelaxed slab. Thus, O atoms were added only on the top of the double-Cr-terminated slab. After relaxation, the slab had a relaxed O-terminated surface on the top and an unrelaxed double-Cr-terminated surfaces at the bottom (Figure 2(c)). The energy of the latter surface is already known from the calculation of the former slab (Figure 2(b)). For these slab structures, the dipole correction [40] in [0001] direction was used to avoid the influence of asymmetry on the energy calculations.

The corrected surface energies are the same as those calculated from totally symmetric slabs containing 8 -Cr-O_3-Cr- monolayers and costing more calculation resources, validating the use of asymmetric slab structures. In the following, the slabs shown in Figure 2 were considered as 1 × 1 unit cells.

The surfaces of Fe_2O_3 have the same crystallographic structures as Cr_2O_3. The only difference comes from the ordering of spins. The relaxed anhydrous surfaces of Fe_2O_3 are shown in Figure S1.

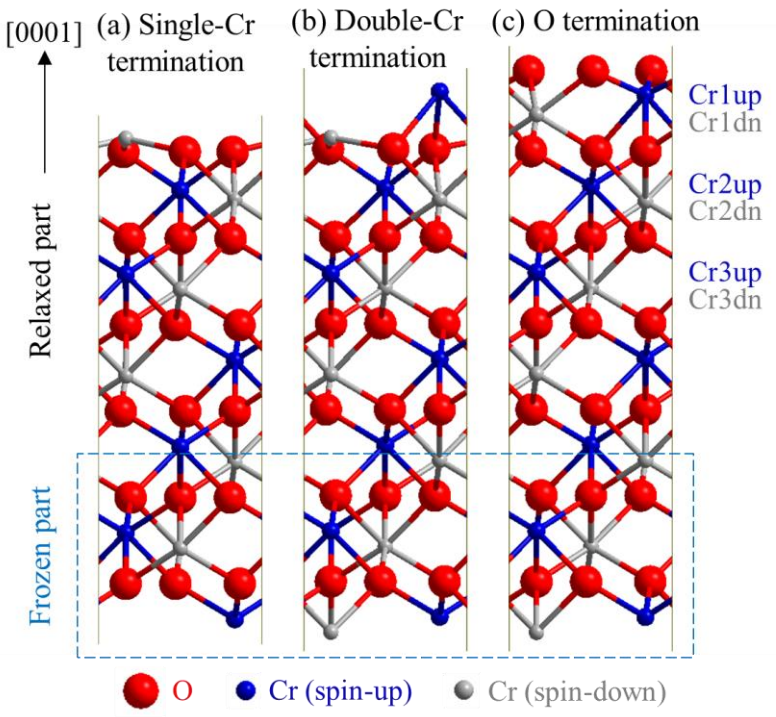

Figure 2. Side views of (0001)-oriented Cr_2O_3 slabs with (a) single-Cr, (b) double-Cr and (c) O terminations on the top relaxed surfaces.

In aqueous solution, H^+ or OH^- from dissociated H_2O can accumulate on polarized surfaces, as discussed in the Introduction section for Fe_2O_3 polarized by external electric field [38], to form hydroxylated surfaces. In an electrochemical process, one can consider that the hydroxyl groups from water adsorbed dissociatively remain on the electrode surface, while the protons are released to the solution, as on the surface polarized by applied external field [38], and the excessive charge is evacuated, forming hydrogen gas on the counter electrode and releasing neutral OH on the surface.

To construct hydroxylated surfaces, neutral hydroxyl groups were added on bare relaxed single- or double-Cr-terminated surface models. Before relaxation, H atoms were placed vertically above (in the [0001] direction) the O atoms that were in the bulk position of O in Cr_2O_3. The structure of the double-Cr-terminated surface fully hydroxylated by hydroxyls (-O_3-Cr_2-$(OH)_3$) is then equivalent to that of the O-terminated surface fully hydroxylated by hydrogen. The

single- and double-Cr-terminated hydrous surface structures will be shown further in the next section.

The fully hydroxylated surfaces (-O_3-Cr_2-$(OH)_3$) contain 3 OH on each 1 × 1 unit cell, corresponding to a surface concentration of 1.4 × 10^{19} m^{-2}. Reducing the number of OH can simulate the cases of lower coverages and the lowest coverage studied in the present work corresponds to one single OH group added on a 2 × 2 supercell. We adopt the following nomenclature (Mμ; k OH; ξ OH/M), where μ is the number of terminating metal atoms in the 1 × 1 unit cell (μ = 1 for single-M-terminated and μ = 2 for double-M-terminated), k the number of OH per unit cell (k = 0.25 for 1 OH in a 2 × 2 supercell, k = 1, 2, 3 respectively for 1, 2 and 3 OH groups in a 1 × 1 unit cell or in each subcell of a 2 × 2 supercell), and ξ the ratio between added OH and terminating metal atoms that bear the OH groups. For example, (M2; 0.25 OH, 0.125 OH/M) refers to the double-M-terminated surface with one OH on each 2 × 2 supercell, bridging two terminating metal atoms and with an overall coverage of OH/M = 0.125.

Generally, to add hydroxyl groups on surfaces, the H atoms are placed vertically above the O atoms before relaxation (i.e., O-H bonds initially along the [0001] direction) but move after relaxation, forming angles between the O-H bonds (called tilted bonds) and the [0001] direction. In the special cases of adding one hydroxyl group on the single-Cr-terminated 1 × 1 unit cell (M1; 1 OH; 1 OH/M) or 2 × 2 supercell (M1; 0.25 OH; 0.25 OH/M), the O and H atoms can be placed vertically above the terminating Cr atom (i.e., Cr-O and O-H bonds parallel to the [0001] direction), forming a Cr-O-H bond normal to the (0001) surface even after surface relaxation. Both configurations are shown in SI (Figure S2). In the present work, both configurations with tilted and normal O-H bonds on single-Cr-terminated surfaces were systematically investigated, and it was found that the structures with tilted bonds are always energetically more favoured than those with normal bonds, even with the presence of substitutional Mo. Thus, only the configuration with tilted O-H bonds will be presented in the following.

The slabs simulated in this work have frozen anhydrous surfaces at the bottom (as shown in Figure 2) and relaxed surfaces on the top with different terminations. The hydroxylation is simulated only on the relaxed top surfaces. With k hydroxyl groups added per unit cell, the chemical formula of the unit cell can be expressed as $\mathrm{Cr_{2n}O_{3(n+m)}} \cdot k\mathrm{OH}$ (n = 6 and m = 0 for single-Cr termination, n = 7 and m = -1 for double-Cr termination and n = 7 and m = 0 for O termination on the top relaxed surfaces for 1×1 unit cells). The cleavage of bulk Cr_2O_3 creates two anhydrous surfaces for each slab and the top surface is hydroxylated by O and H atoms from the environment. To be able to compare directly the stability of surfaces of different terminations, the free energy of relaxed top surfaces γ_{top} can be calculated as

$$\gamma_{\mathrm{top}} = \frac{1}{A}\left[E_{\mathrm{Cr_{2n}O_{3(n+m)}}\cdot k\mathrm{OH(slab)}} - nE_{\mathrm{Cr_2O_3(bulk)}} - (3m+k)\mu_{\mathrm{O}} - k\mu_{\mathrm{H}}\right] - \gamma_{\mathrm{bot}} \qquad (1)$$

where A is the unit cell area of the (0001)-oriented slab, the second and third terms the DFT energies of optimized slab and of bulk Cr_2O_3, respectively, and μ_{O} and μ_{H} the chemical

potentials of O and H, respectively. γ_{bot}, the free energy of the frozen bottom surface, can be calculated using the DFT energy of unoptimized anhydrous slabs:

$$\gamma_{\mathrm{bot}} = \frac{1}{2A}\left[E_{\mathrm{Cr_{2n}O_{3(n+m)}(slab,unopt)}} - nE_{\mathrm{Cr_2O_3(bulk)}} - 3m\mu_{\mathrm{O}}\right]. \quad (2)$$

The most stable surface structure has the lowest surface free energy. The difference of energies between an anhydrous surface and a hydrous surface gives the energy necessary to hydroxylate the anhydrous surface. The chemical potentials used in Equations (1) and (2) can be expressed depending on the environments where the hydroxylation occurs (i.e. depending on the references we choose for the adsorbed O and H atoms). Three possible choices are discussed in Appendix A, and we will investigate the surfaces in these environments.

To study the effects of Mo, one cation in the 1 × 1 unit cell or four cations at the same site of the same plane in the 2 × 2 supercell were replaced by Mo. This allowed us to simulate substitutional Mo at high surface concentration, noted as 1 Mo per unit cell. The substitution is performed only on the top surfaces of slabs since the bottom surfaces are frozen. Different sites of cations from the surface to the bulk (shown in Figure 2) can be substituted by Mo. One cation in the 2 × 2 supercell was replaced by Mo to simulate Mo at low surface concentration, noted as 0.25 Mo per unit cell. Adding 1 ~ 3 OH per unit cell was then simulated with 1 × 1 unit cell for hydrous surfaces without or with 1 Mo per unit cell, and with 2 × 2 supercell for surfaces with 0.25 Mo per unit cell (with the same numbers and initial configurations of OH in each sub-cell).

For a slab with *s* substitutional Mo per unit cell, the chemical formula per unit cell can be written as $\mathrm{Cr_{2n-s}Mo_sO_{3(n+m)}} \cdot k\mathrm{OH}$. The chemical potentials of Cr and Mo are approximated by the DFT energies of the corresponding pure metals $E_{\mathrm{Cr(bulk)}}$ and $E_{\mathrm{Mo(bulk)}}$, respectively. The energy of substitution of one metal cation by one Mo E_{sub} can be calculated by the following expression:

$$E_{\mathrm{sub}} = \frac{1}{s}\Big(E_{\mathrm{Cr_{2n-s}Mo_sO_{3(n+m)}}\cdot k\mathrm{OH(slab)}} - E_{\mathrm{Cr_{2n}O_{3(n+m)}}\cdot k\mathrm{OH(slab)}} + sE_{\mathrm{Cr(bulk)}} - sE_{\mathrm{Mo(bulk)}}\Big). \quad (3)$$

Fe_2O_3 surfaces were treated in the same way as Cr_2O_3 surfaces. The vibrational entropy and zero-point energy contributions to the free energy of surface formation and cation substitution were omitted, so the energies of slabs and bulk involved in the above equations were approximated by the DFT energies. Most of the calculation details were presented in our previous work [8], for structures without H. For H, the standard version of pseudopotential was chosen, and no initial magnetic moment was distributed to H when calculating hydrous oxide surfaces.

Bader charge analysis [44] was performed to investigate the charge state of atoms. As shown in our previous work [8], Cr (Fe) in bulk Cr_2O_3 (Fe_2O_3) had a Bader charge of +1.8 *e* and O a Bader charge of -1.2 e, indicating a ratio of 0.6 between Bader charges and formal charges. This ratio was used in the present work to convert Bader charges to formal charges.

All considered models and optimized structures were built and visualized using the Modelview visualization software developed by B. Diawara [45].

3. Results and discussion

3.1. Surfaces without Mo

In this section, anhydrous surfaces are presented first, followed by hydrous surfaces to identify the most stable surface structure in the conditions of interest.

3.1.1. Anhydrous surfaces

Three types of anhydrous surface terminations (shown in Figure 2) were simulated in the present work. They can transform between them by adsorbing/releasing O from/to the environment. Figure 3 shows the surface free energy for Cr_2O_3 surfaces as a function of oxygen chemical potential. Since only anhydrous surfaces are investigated in this section, the oxygen chemical potential can be expressed for dry gaseous environment using Equation (4). The anhydrous surface cannot be double-Cr-terminated without dissociation of Cr_2O_3 into Cr, as indicated by the vertical green dashed line in Figure 3. The O potential at which the dissociation occurs is determined from the experimental value of the formation free energy of Cr_2O_3 [41]. Based on Equation (1), the free energy of the O-terminated surface is lower than that of the single-Cr-terminated surface at high oxygen partial pressures. The intersection point is similar to that calculated by Rohrbach *et al*. [20]. In air (vertical pink dashed line in Figure 3), the free energy of the O-terminated surface, lower than that of the single-Cr-terminated surface, suggests that Cr_2O_3 films in dry air may have O termination.

For Fe_2O_3, the single-Fe-terminated surface is always the most stable between the O chemical potential limits for oxide dissociation and air. The surface free energies are shown in SI (Figure S3).

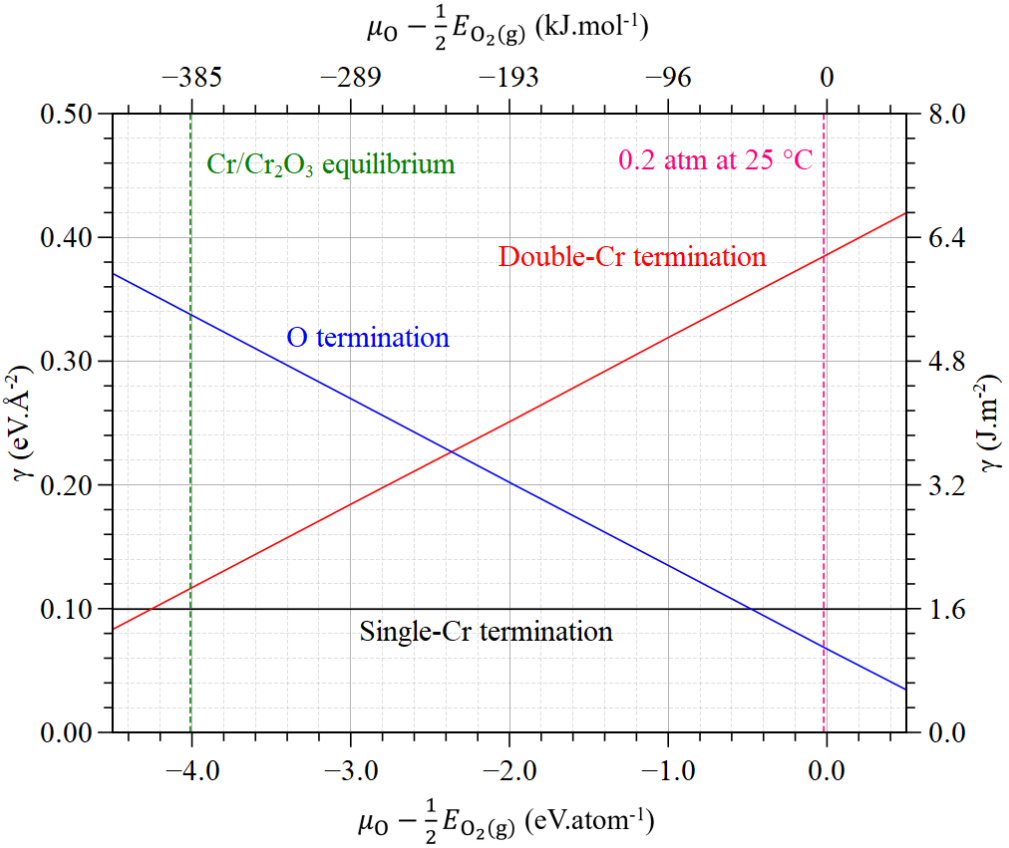

Figure 3. Surface free energies of different (0001)-oriented anhydrous Cr_2O_3 surface terminations.

Figure 4 shows the charges on the atoms for Cr_2O_3 surfaces with different terminations relative to charges in the bulk. For the single-Cr-terminated surface, the decrease of charge due to surface formation is negligible (maximum decrease of 0.2 *e* in formal charge for the terminating Cr), suggesting that the terminating Cr is still in +3 oxidation state. For the double-Cr-terminated surface, the decrease of formal charge is 1.8 *e* for the "Cr1up" and 0.8 *e* for "Cr1dn" atoms, indicating that the Cr atoms terminating the surface are in about +1 and +2 oxidation states, respectively. For the O-terminated surface, the formal charges of the terminating O and the "Cr1up" on subsurface increase by 0.7 and 0.5 e, respectively. In this case, one can roughly consider that the terminating O is in near -1 oxidation state and the underneath "Cr1up" atom in near +3 oxidation state. In bulk Cr_2O_3, the stable oxidation states should be +3 for Cr and -2 for O. It suggests that for the double-Cr- and O-terminated surfaces, the electrons localized on the terminating Cr and O atoms are in excess and in depletion, respectively, compared to the atoms in their stable oxidation states.

The double-Cr- and O-terminated surfaces were simulated by considering chemical stoichiometric (Figure 2.b)) and non-stoichiometric slabs (Figure 2(c)), respectively, that both contain an unrelaxed double-Cr-terminated surface at the bottom. We found that the charge distributions are the same for both unrelaxed surfaces of the slabs, suggesting that the charge variations on the double- and O-terminated surfaces were not an artefact from the slab models.

Calculations with symmetric slab models that contain both relaxed surfaces on the top and at the bottom yields the same surface energies and charge distributions. Interaction between the surfaces on both sides of slabs was not observed since the variation of charges on the subsurface near bulk zone was negligible. Thus, the charge changes on the terminating atoms may only come from their reduced coordination.

Fe_2O_3 surfaces yielded similar charge distributions as Cr_2O_3, which are shown in SI (Figure S4).

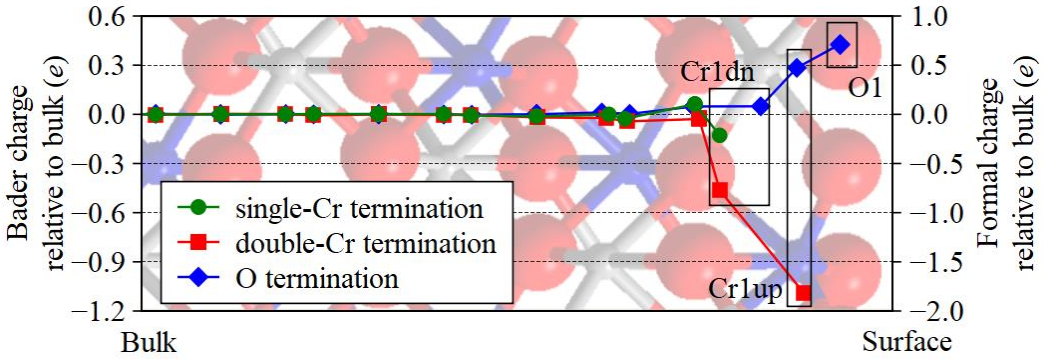

Figure 4. Bader and formal charges relative to bulk for anhydrous (0001)-oriented Cr_2O_3 surfaces with different terminations. Each point represents an atomic layer whose nature is indicated by the background image of the perfect surface according to the [0001] coordinate. O atoms are in red and metal atoms in grey and blue.

3.1.2. Hydrous surfaces

Single-M- and double-M-terminated surfaces hydroxylated by hydroxyls are investigated in this section. The O-terminated surface fully hydroxylated by hydrogen is equivalent to double-Cr-terminated surface fully hydroxylated by hydroxyls in terms of surface structure. Different configurations denoted by (Mμ; k OH; ξ OH/M) as defined in the Methods section are discussed hereafter.

Figure 5 and Figure 6 show the structures of hydroxylated single- and double-Cr-terminated surfaces, respectively. On the single-Cr-terminated (M1; 0.25 OH; 0.25 OH/M) and (M1; 1 OH; 1 OH/M) surfaces with a low degree of hydroxylation, the O atom of the OH groups, initially in the bulk position of O in Cr_2O_3, moved above the terminating Cr after surface relaxation, while on the double-Cr-terminated (M2; 0.25 OH; 0.125 OH/M) and (M2; 1 OH; 0.5 OH/M) surfaces they stayed in the initial position of O in Cr_2O_3. On the surfaces with a high degree of hydroxylation (2 ~ 3 OH), the hydroxyl groups form H-bond networks, zig zag or circular, on both single- and double-Cr-terminated surfaces as shown by green rectangles and circles in the top views of Figure 5 and Figure 6).

The structures of hydrous Fe_2O_3 surfaces are similar to those of Cr_2O_3, except for the double-Fe-terminated (M2; 0.25 OH; 0.125 OH/M) surface with a low degree of hydroxylation on

which an O atom on the surface moves toward the terminating Fe atomic plane. The detailed structure is shown in SI (Figure S5).

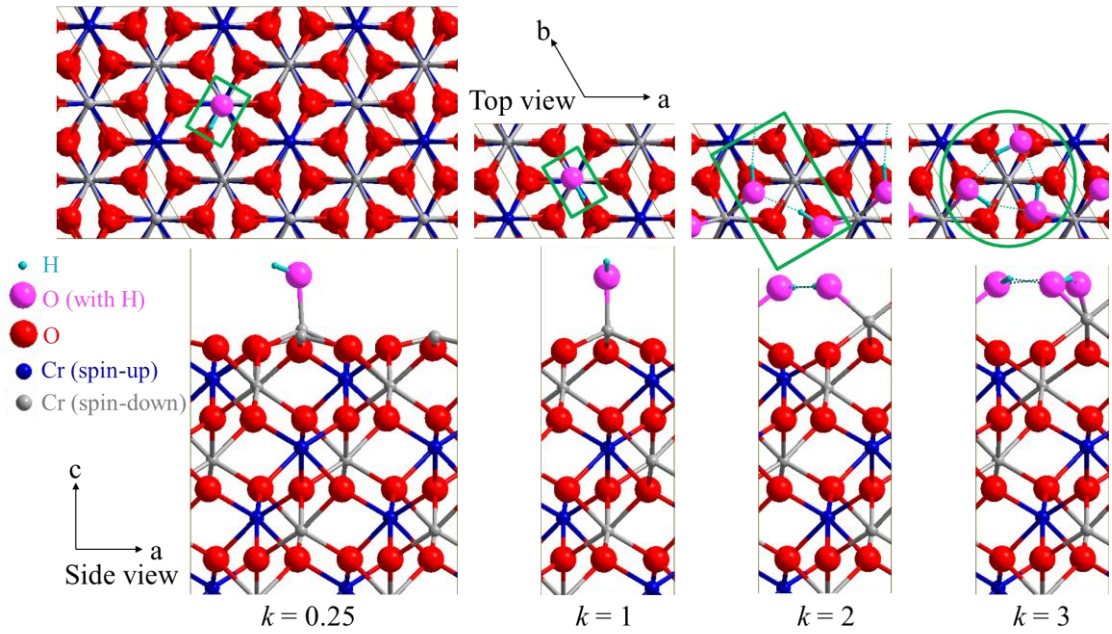

Figure 5. Top and side views of hydrous (0001)-oriented single-Cr-terminated (M1; *k* OH; *k* OH/M) Cr_2O_3 surfaces.

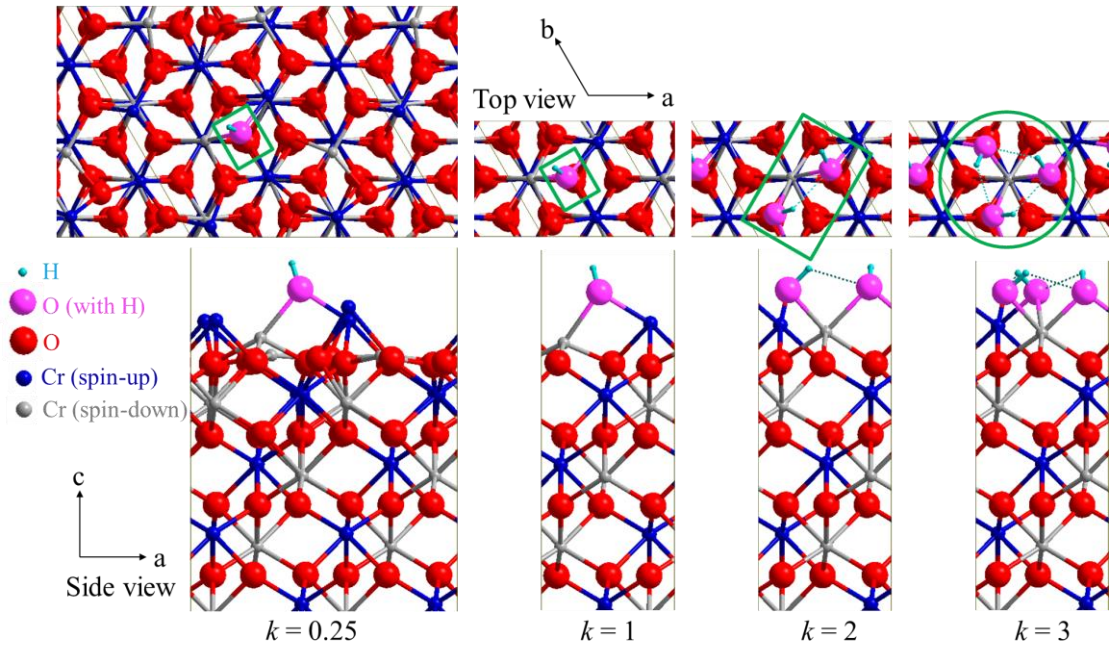

Figure 6. Top and side views of hydrous (0001)-oriented double-Cr-terminated (M2; *k* OH; *k*/2 OH/M) Cr_2O_3 surfaces.

To study the surface stability in different environments (temperature, partial pressures, hydroxylation in solution, etc.), the most stable surface with the lowest energy was determined

at different O and H chemical potentials. Figure 7(a) shows the resulting phase diagram of Cr_2O_3 at 25 °C. In gaseous environment, the H potential is proportional to the H_2O potential according to Equation (6). In air at 25 °C (horizontal red dashed line in Figure 7(a)), the free energies of O-terminated bare surface, single-Cr-terminated surface with a low degree of hydroxylation (M1; 1 OH; 1 OH/M) and fully hydroxylated double-Cr-terminated surface (M2; 3 OH; 1.5 OH/M) are the lowest at relatively low, intermediate (sufficient to hydroxylate the surfaces) and high H_2O partial pressure, respectively. In extremely humid environments like in water-saturated gases (intersection point of the black and red lines in Figure 7(a)), the Cr_2O_3 surface will be fully hydroxylated and double-Cr-terminated. In the cases where the surface is hydroxylated in solution (by liquid water and dissolved oxygen or by electrochemical process, shown by the black dashed line in Figure 7(a)), it also will be always fully hydroxylated with double-Cr-termination between the O potential limits. The free energies of hydroxylated surfaces in the case of electrochemical process at pH = 0 and 25 °C are shown in SI (Figure S6).

Figure 7(b) shows the surface stability diagram for Fe_2O_3. The most stable surface is also fully hydroxylated double-M-terminated surfaces ($-O_3-Fe_2-(OH)_3$) in the oxidant zone, whereas the surface will release one OH in relatively reductive conditions to become $-O_3-Fe_2-(OH)_2$. The surface free energies are shown in SI (Figure S7).

This surface stability study suggests that immersing Cr_2O_3 from dry air into aqueous solutions at room temperature will transform the surface from O-terminated anhydrous state ($-Cr_2-O_3$) to fully hydroxylated state ($-O_3-Cr_2-(OH)_3$), while immersing Fe_2O_3 will hydroxylate the single-Fe-terminated anhydrous surface state ($-O_3-Fe$) to ($-O_3-Fe_2-(OH)_2$) or ($-O_3-Fe_2-(OH)_3$) surface state. Both formation mechanisms are different from direct adsorption of neutral hydroxyl on double-M-terminated surfaces, but the final structures are the same.

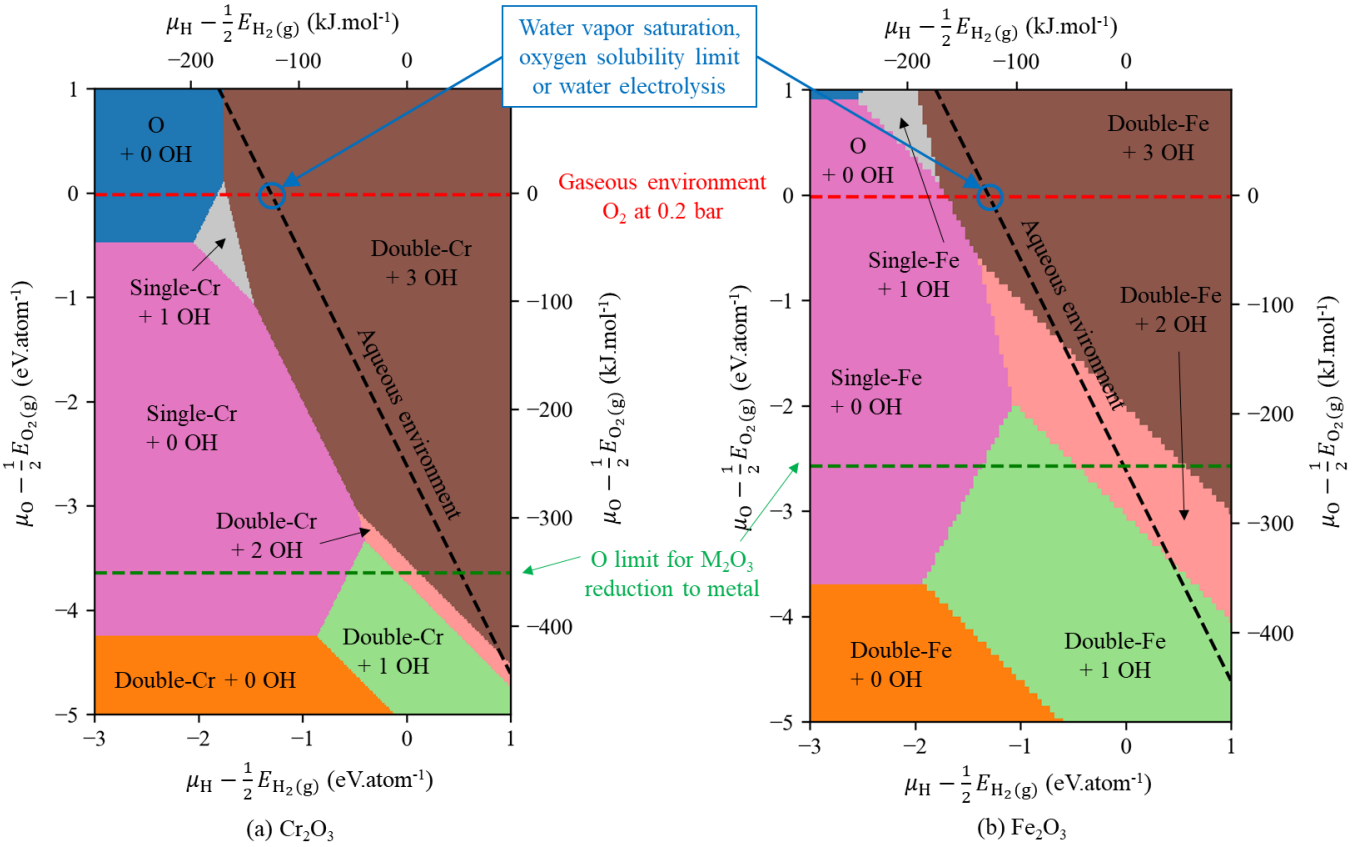

Figure 7. Phase diagram at 25 °C for anhydrous and hydrous (0001)-oriented (a) Cr_2O_3 and (b) Fe_2O_3 surfaces. Termination and number of added hydroxyl groups are indicated. The red, black and green lines represent the environments in air, in water-saturated gas or aqueous solutions and at Cr/Cr_2O_3 equilibrium, respectively.

Figure 8 shows the changes of charges on Cr_2O_3 surfaces resulting from the addition of OH groups. The charges are relative to the bare surfaces except for adsorbed OH groups for which full charges are shown. The formal charges of O and H in OH groups are basically -2 and +1 *e*, indicating that each neutral added OH group releases one positive charge on Cr_2O_3 surfaces. On double-Cr-terminated surfaces (Figure 8(b)), the charges released from the OH groups are localized on two terminating Cr atoms. The charges provided by the first (M2; 0.25 ~ 1 OH; 0.125 ~ 0.5 OH/M) and second OH are localized on the "Cr1up" atom, and that from the third OH on "Cr1up" and "Cr1dn" atoms. On single-Cr-terminated surfaces (Figure 8(a)), the released charges are firstly localized on the terminating Cr for the surfaces with a low degree of hydroxylation (M1; 0.25 ~ 1 OH; 0.25 ~ 1 OH/M) and then on the subsurface Cr ("Cr2up") for the surfaces with a high degree of hydroxylation (M1; 2 ~ 3 OH; 2 ~ 3 OH/M). These trends are similar to those on Fe_2O_3 hydrous surfaces.

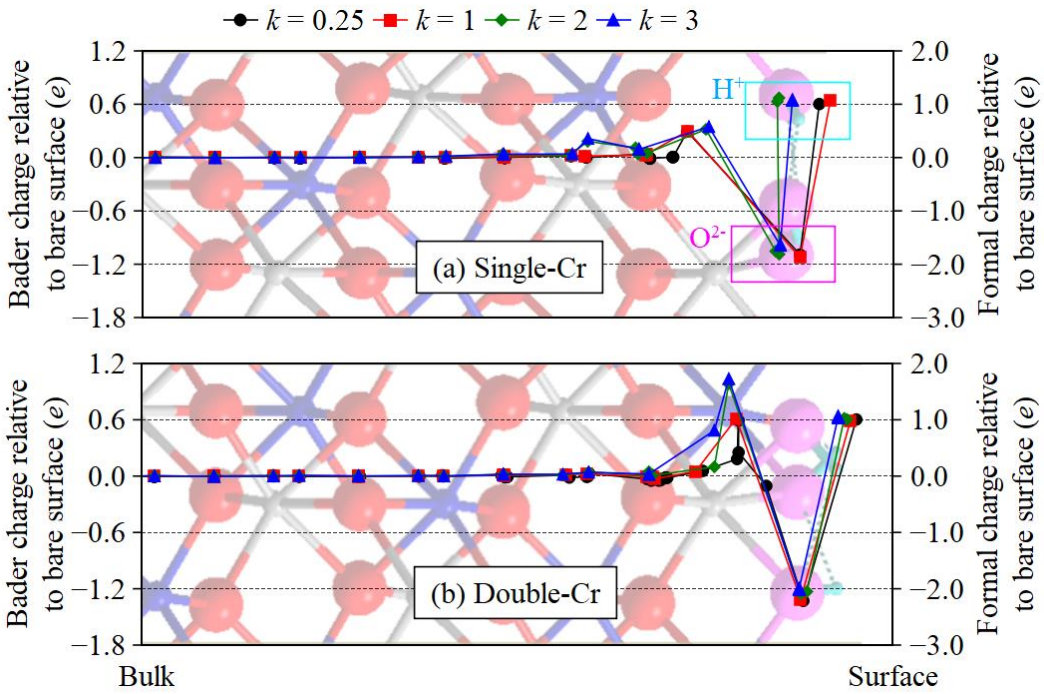

Figure 8. Bader and formal charge changes induced by OH adsorption on (0001)-oriented Cr_2O_3 surfaces: (a) single-Cr (M1; *k* OH; *k* OH/M) and (b) double-Cr-terminated (M2; *k* OH; *k*/2 OH/M). The full charges are shown for the OH groups. Each point represents an atomic layer whose nature is indicated by the background image of the surface according to the [0001] coordinate. O atoms are in red (for oxide) and magenta (for OH groups), metal atoms in blue (spin-up) and gray (spin-down), and H atoms in cyan.

Table 1 compiles the formal charge of the terminating atoms ("M1up" and "M1dn") for single- and double-M-terminated surfaces to better determine their oxidation states. For single-M-terminated surfaces, the terminating atoms are always in +3 oxidation state before and after the addition of OH (providing positive charges), suggesting that the maximal oxidation state of Cr(Fe) is +3 on surfaces with corundum structure. On the bare double-M-terminated surface, the terminating "M1up" and "M1dn" atoms are in +1 and +2 oxidation state, respectively. The surface addition of the first OH group (M2; 0.25 ~ 1 OH; 0.125 ~ 0.5 OH/M) increases the oxidation state of the "M1up" atoms to +2, matching that of the "M1dn" atoms. The charges from the second and third OH groups (M2; 2 ~ 3 OH; 1 ~ 1.5 OH/M) further increase the oxidation states of both terminating atoms to +3. The lack of localized positive charge on the bare double-M-terminated surface is filled just enough in the fully hydroxylated state to keep Cr(Fe) and O in their stable oxidation states.

Table 1. Formal charges of terminating Cr(Fe) atoms on (0001)-oriented Cr_2O_3 and Fe_2O_3 surfaces. For (M1; 0.25 OH; 0.25 OH/M) and (M2; 0.25 OH; 0.125 OH/M), only the Cr atoms bonded to OH groups are considered.

Number of OH	Single-Cr	Single-Fe	Double-Cr		Double-Fe	
per unit cell	Cr1dn	Fe1dn	Cr1up	Cr1dn	Fe1up	Fe1dn

0	2.8	2.7	1.2	2.2	1.4	1.9
0.25	3.2	2.8	2.1	2.3	2.2	2.1
1	3.3	2.9	2.2	2.3	2.2	2.2
2	3.3	3.0	2.8	2.3	2.3	2.9
3	3.3	3.1	2.9	3.0	3.0	3.0

3.2. Cr_2O_3 surfaces with Mo

In the following, Mo incorporation on Cr_2O_3 surfaces by substituting surface and subsurface cations is presented. Firstly, surfaces with one Mo per unit cell, which is a high surface concentration of substitutional atoms, are considered and the most stable substitution sites for different surface terminations and OH coverages are determined. Secondly, substitution with a relatively low Mo concentration (i.e., 1 Mo per 2 × 2 supercell) is considered and the optimal surface structures are discussed.

3.2.1. Substitution with high Mo concentration

Cr located on the different sites of Cr_2O_3 surfaces labelled in Figure 2 was replaced by Mo to investigate the most stable site for substitution. One substitutional Mo per unit cell was added on anhydrous and hydrous surfaces for the tests. Substitution by Mo did not significantly change the surface structures.

Figure 9 shows the energies of substitution by Mo obtained for the tested Cr sites and surface terminations. On single-Cr-terminated surfaces (Figure 9(a)), the preferential site for substitutional Mo is in the subsurface ("Cr2dn") in the absence of surface OH group, but on the surface ("Cr1dn") in presence of any added OH. On double-Cr-terminated surfaces (Figure 9(b)), the most stable site is in depth ("Cr3dn") on the anhydrous surface. With one OH added per unit cell (M2; 1 OH; 0.5 OH/M), the most stable site is in the subsurface ("Cr2dn"), and as the surface becomes more hydroxylated (M2; 2 ~ 3 OH; 1 ~ 1.5 OH/M), the "Cr1dn" surface site becomes the most stable for substitution by Mo (only the (M2; 3 OH; 1.5 OH/M) case is shown in Figure 9(b) for the sake of clarity). On bare O terminated surface, "Cr1up" is the favoured substitutional site for Mo. These data show that whereas the preferential site for substitutional Mo is on the subsurface in anhydrous conditions, it is on the surface when the surfaces have a high degree of hydroxylation, in agreement with the experimental observations on passive films [6] that indicate that Mo (IV) is concentrated at the interface between the inner Cr-rich oxide layer and the outer hydroxide layer.

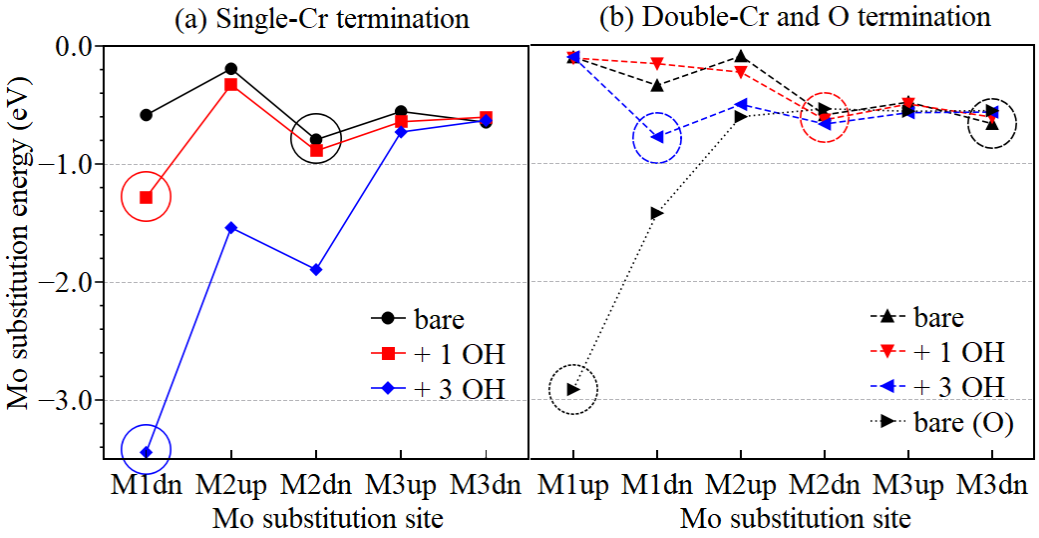

Figure 9. Energy of substitution by Mo on different cations sites for bare (anhydrous) and OH-covered (0001)-oriented Cr_2O_3 surfaces (substitution with high Mo concentration) with (a) single-Cr, (b) double-Cr and O terminations. The most stable sites are marked by circles.

Figure 10 shows the Bader and formal charges of Mo in different substitution sites for different surface terminations and OH coverages. In the cases of anhydrous double- and single-Cr-terminated surfaces and the double-Cr-terminated surface with a low degree of hydroxylation (M2; 1 OH; 0.5 OH/M) for which the most stable site of substitutional Mo is in the subsurface, the charge of the substitutional Mo is lower for substitution on the surface sites ("Cr1up" and "Cr1dn") than in the subsurface sites, which are near 3 *e*. In the other cases of higher hydroxylation, the substitutional Mo has a higher charge on the surface than in the subsurface, suggesting that the free positive charges on these surfaces are in excess and can be localized on the substitutional Mo while keeping Cr and O in +3 and -2 oxidation states, respectively. The consistency for the trends of localized charge and substitution energy implies that the substitutional Mo tends to have higher localized charge.

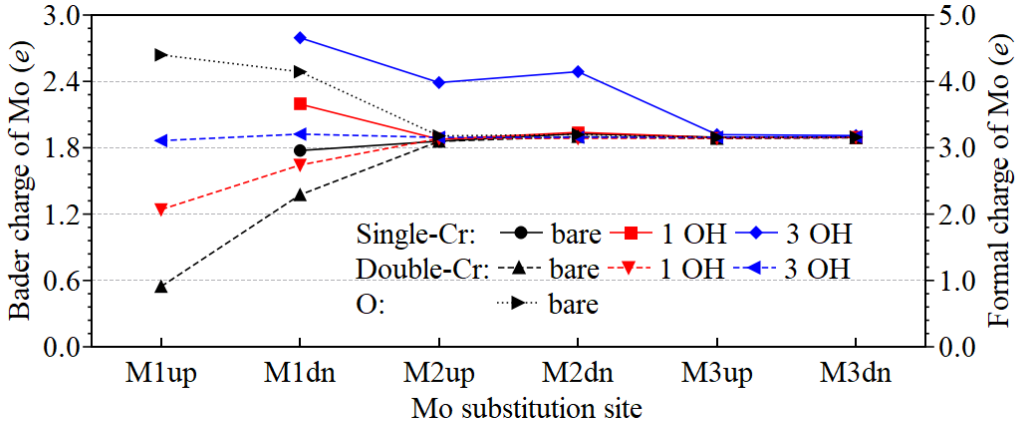

Figure 10. Bader and formal charges of substitutional Mo on different cations sites for bare (anhydrous) and OH-covered (0001)-oriented Cr_2O_3 surfaces (substitution with high Mo

concentration).

Table 2 summarizes the results. It appears clearly that the presence of OH groups favours the location of Mo at the interface between oxide and surface OH layer. Whereas formal charge localized on Mo varies little with Mo location on double-Cr-terminated surfaces, it increases with OH loading on single-Cr-terminated surfaces.

Table 2. Most stable substitution site and formal charge for substitutional Mo for bare (anhydrous) and OH-covered (0001)-oriented Cr_2O_3 surfaces (substitution with high Mo concentration).

OH number	Single-Cr		Double-Cr		O termination	
per unit cell	Mo location	charge	Mo location	Charge	Mo location	charge
0	Cr2dn	+ 3.2	Cr3dn	+ 3.2	Cr1up	+ 4.4
1	Cr1dn	+ 3.7	Cr2dn	+ 3.1		
3	Cr1dn	+ 4.7	Cr1dn	+ 3.2		

In the following, substitutional Mo is considered in the most stable sites for each type of studied surface: the substituted site is “M3dn” for double-M-terminated anhydrous surfaces, “M2dn” for single-M-terminated anhydrous surfaces and double-M-terminated surfaces with a low degree of hydroxylation (M2; 0.25 ~ 1 OH; 0.125 ~ 0.5 OH/M), “M1dn” for all single-M-terminated hydrous surfaces (M1; 0.25 ~ 3 OH; 0.25 ~ 3 OH/M) and double-M-terminated surfaces with a high degree of hydroxylation (M2; 2 ~ 3 OH; 1 ~ 1.5 OH/M), and “M1up” for O-terminated surfaces.

The substitutions by 1 Mo per unit cell are always exothermic, as shown in Figure 9, suggesting that the Mo-substituted surfaces are more stable than the non-substituted ones for the same surface termination. In order to investigate the surface stability after substitution by Mo and to compare to that without Mo substitution (Figure 7), a phase diagram was calculated only considering the surfaces with 1 Mo per unit cell; it is shown in Figure 11(a). The DFT energy of bulk Cr_2O_3 with one substitutional Mo per unit cell was used in Equation (1). Whereas the bare O-terminated surface is favoured in more oxidant conditions, the double-Cr-terminated surface with full OH coverage (M2; 3 OH; 1.5 OH/M) is still the most stable structure for hydrous surfaces in aqueous environments between the O limits.

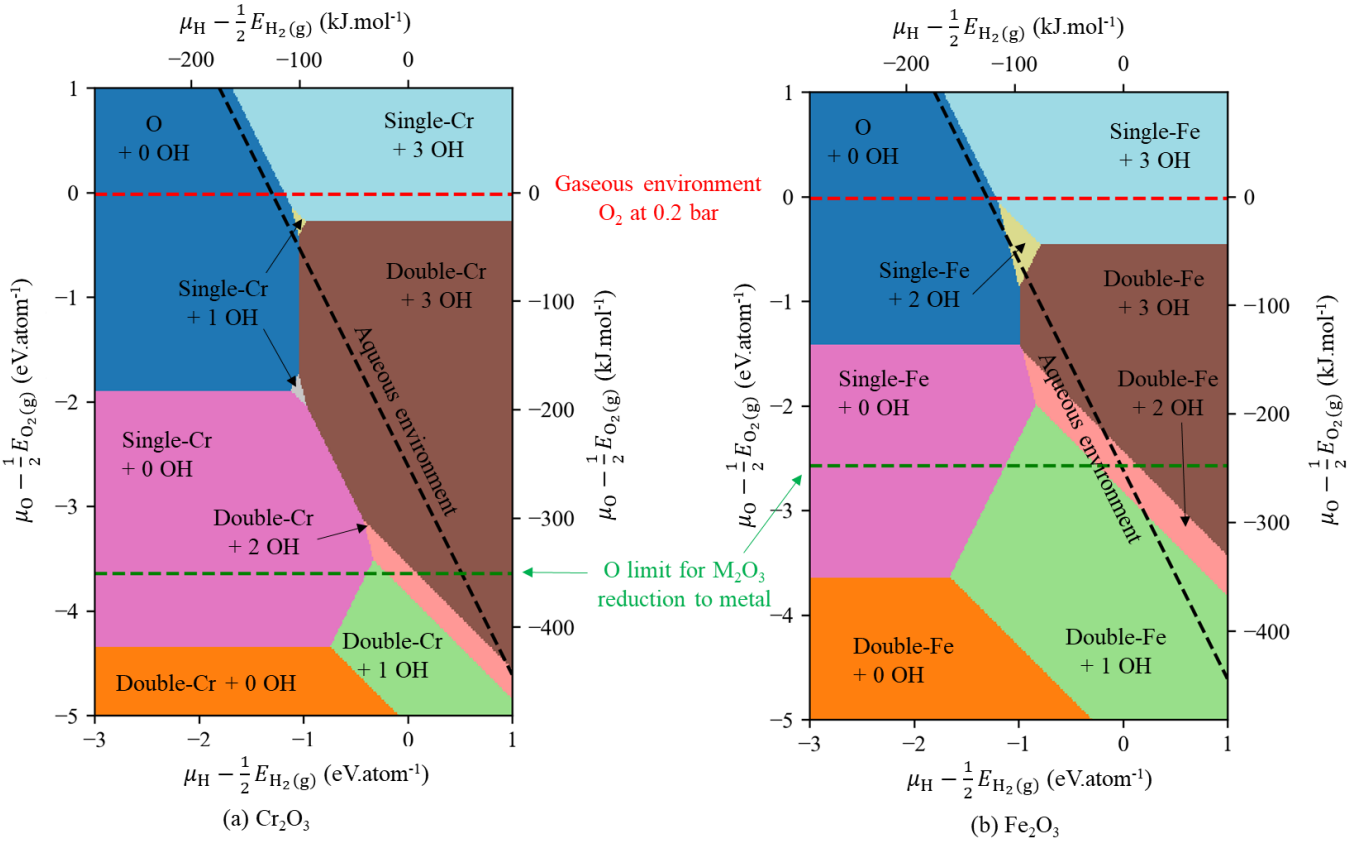

Figure 11. Phase diagram at 25 °C of Mo-substituted anhydrous and hydrous (0001)-oriented (a) Cr_2O_3 and (b) Fe_2O_3 surfaces (substitution with high Mo concentration). The termination and the number of added hydroxyl groups are indicated. The red, black and green lines represent the environments in air, in water-saturated gas or aqueous solutions and at Cr/Cr_2O_3 equilibrium, respectively.

3.2.2. Substitution with lower Mo concentration

For substitution by 0.25 Mo per unit cell (i.e. one Mo per 2 × 2 supercell), several configurations of OH-covered single-Cr-terminated surfaces were tested. In the case of one OH added per 2 × 2 supercell (M1; 0.25 OH; 0.25 OH/M), configurations with the OH group above the substitutional Mo or above the other unsubstituted "Cr1dn" atoms were tested. The surface cell with the OH group bonded on Mo site is the most energetically stable, suggesting that the substitutional Mo is easier to hydroxylate than the "Cr1dn" atoms which are in stable +3 oxidation state. In the case of 4 OH groups added per 2 × 2 supercell (M1; 1 OH; 1 OH/M), the surface with all OH bonds tilted in the same orientation is more stable than that with OH bonds tilted in different orientations. For fully hydroxylated surfaces (M1; 3 OH; 3 OH/M), the OH network becomes less regular on the Mo-substituted surface than on the Mo-free surface (Figure 5). Figure 12 shows this structure with the OH network (green triangle and circle) influenced by the substitutional Mo. Other structures are not shown since not altered by substitutional Mo. For double-Cr-terminated surfaces with 0.25 substitutional Mo per 2 × 2 supercell, the

structures are not shown here since they are similar to those of surfaces without Mo.

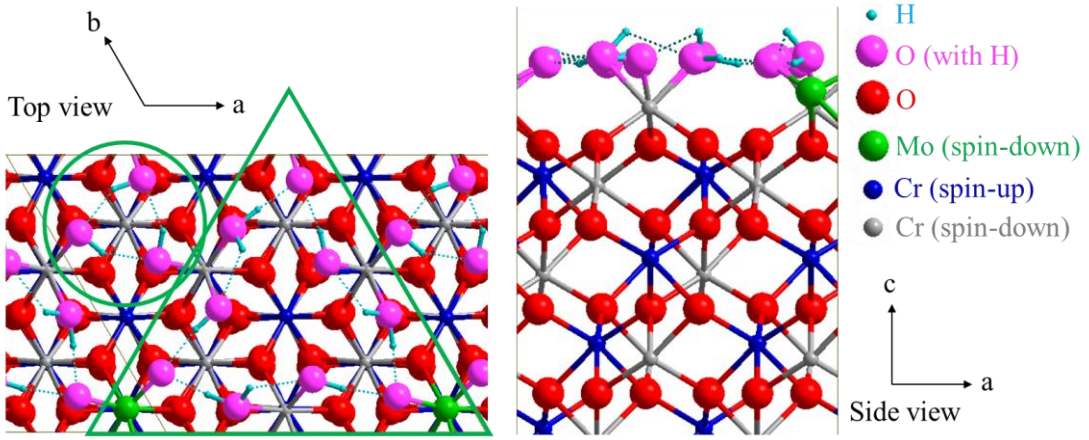

Figure 12. Top and side views of fully hydroxylated (0001)-oriented Cr_2O_3 surface single-Cr-terminated (M1; 3 OH; 3 OH/M) with 0.25 Mo per unit cell.

3.3. Cr_2O_3 vs Fe_2O_3 surfaces with Mo

Anhydrous and OH-covered Fe_2O_3 surfaces substituted by Mo were also investigated. The substitution sites were verified on the fully hydroxylated double-Fe-terminated surfaces with 1 substitutional Mo per unit cell. The substitution energies are shown in SI (Figure S8) and the same site ("M1dn") was found the most stable for substitution. Thus, the same substitution sites determined for Cr_2O_3 surfaces (Table 2) were used for substituted Fe_2O_3 surfaces. No significant alteration of the surface structures was observed resulting from substitution by Mo, like on the Cr_2O_3 surfaces. Figure 13 shows the energy of substitution by Mo on Cr_2O_3 and Fe_2O_3 surfaces without and with different coverages of OH. The DFT energies used to calculate these substitution energies are provided in SI (Table S1). Some substitution energies in Figure 13 are remarkably low (ex. -7.63 eV for the anhydrous Fe_2O_3 surface (M2; 1 OH; 0.5 OH/M) with 0.25 Mo per unit cell).

On single-M-terminated surfaces, a higher Mo concentration yields a decrease of the energy gain brought by substitution for both Cr_2O_3 and Fe_2O_3 surfaces, probably due to the repulsion between substitutional Mo atoms. However, at high concentration (i.e., 4 Mo per 2 × 2 supercell), all substitutional Mo are constrained in the same plane (same substitution site in unit cell). Tests with other configurations in which Mo would substitute sites in different cation planes were not conducted. The negative energy of substitution by Mo decreases (i.e., substitution is more favoured) with increasing OH coverage, except for two Fe_2O_3 surfaces: (M1, 0.25 OH, 0.25 OH/M) with 1 Mo per unit cell and (M1, 3 OH, 3OH/M) with 0.25 Mo per unit cell. This suggests that the presence of Mo will promote full hydroxylation of single-M-terminated surfaces.

As for double-M-terminated surfaces, the energies of substitution by Mo at low concentration

(0.25 Mo per unit cell) are markedly lower on anhydrous and fully hydroxylated than on the other OH-covered surfaces, whilst on surfaces with a high concentration of substitutional Mo (1 Mo per unit cell), the influence of OH coverage on the substitution energy is less marked.

Comparing the single- and double-M-terminated hydrous surfaces, the energies of substitution are lower for the single-M-terminated hydrous surfaces of Fe_2O_3 and Cr_2O_3 regardless of OH coverage, indicating a stabilization of the single-M-terminated surfaces by the substitution by Mo. On Cr_2O_3 surfaces, the double-Cr termination with full OH coverage (M2; 3 OH; 1.5 OH/M) is still the most stable hydrous surfaces in the range of interest as shown in Figure 11, even if single-Cr-terminated surfaces are more favoured by the substitution by Mo (Figure 13). On Fe_2O_3 surfaces, besides the fully hydroxylated double-Fe-terminated surface, the single-Fe-terminated surface (M1; 2 OH; 2 OH/M) can also be stable in aqueous solution, due to the stabilization by substitutional Mo. A diagram of surface stability for Fe_2O_3 is shown in Figure 11(b).

The substitution by Mo is exothermic on both Cr_2O_3 and Fe_2O_3 surfaces. The energy of substitution is (slightly) lower on Cr_2O_3 than on Fe_2O_3 surfaces only in the case of the fully hydroxylated single-M termination with low Mo loading, which is not the most favoured surface configuration based on the surface stability diagrams (Figure 7 and Figure 11). Except for this single case, the energies of substitution on Fe_2O_3 surfaces are more negative than those on Cr_2O_3 surfaces, suggesting preferential substitution by Mo in Fe- than Cr-rich oxide zones of the inner barrier layer of passive films. In our previous study [8], it was found that the presence of substitutional Mo favours and disfavours the formation of metal and O vacancies, respectively, thereby curing the Fe-rich weak sites of passivity and enhancing the resistance to passivity breakdown in chloride-rich environment. In the present work, we confirm that substitution by Mo is exothermic and more favoured on hydroxylated Fe oxide than on Cr oxide surfaces, further supporting the mechanisms of Mo-enhanced passivity previously proposed [9].

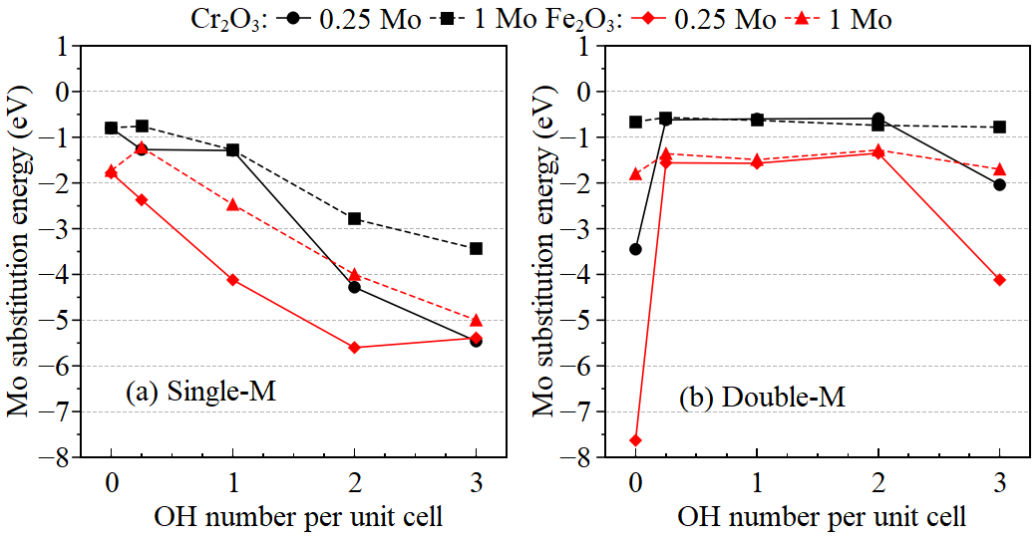

Figure 13. Energy of substitution by Mo at low (0.25 Mo per unit cell) and high (1 Mo per

unit cell) concentration on (0001)-oriented Cr_2O_3 and Fe_2O_3 surfaces (a) single-M- and (b) double-M-terminated with increasing OH surface concentration.

Figure 14 shows the formal charge localized on Mo (on substituted surface) or on the un-substituted atom (at 0 Mo surface concentration) for single-M-terminated surfaces. The formal charges of Mo on double-M-terminated surfaces are not shown, since they are always near 3 *e*, regardless of the OH coverage.

The formal charges of the substituted Cr(Fe) atoms are close to 3 *e* on surfaces without Mo regardless of the OH coverage, like those of substitutional Mo on anhydrous surfaces regardless of the Mo concentration. However, the formal charge on substitutional Mo increases to a higher level once the surfaces are hydroxylated by adsorbing OH. At a surface loading of 0.25 Mo per unit cell, the Mo charge increases to 3.7 *e* for intermediate OH coverage and becomes higher (4.4 ~ 4.6 *e*) at higher OH coverage. This trend is even more pronounced at higher Mo surface loading (1 Mo per unit cell forming -O_3-Mo-$(OH)_{1\sim3}$ terminations): Mo formal charge from 3.7 to 4.2 and then to 4.7 *e* as OH coverage increases. The Mo formal charge in Fe or Cr oxide matrices are similar except for the case (M1; 1 OH; 1 OH/M) with 0.25 Mo loading per unit cell in which the Mo charge is higher in Fe than in Cr oxides. With higher OH coverage, more charges released by the OH groups are localized on Mo, resulting in the substitutional Mo at +4 or higher oxidation state. Again, this is consistent with the experimental observations by XPS on passive films [6], in which Mo was measured at +4 oxidation state at the interface between outer hydroxide and inner oxide layers and at intermediate oxidation state between +4 and +6 deeper, in the inner barrier layer.

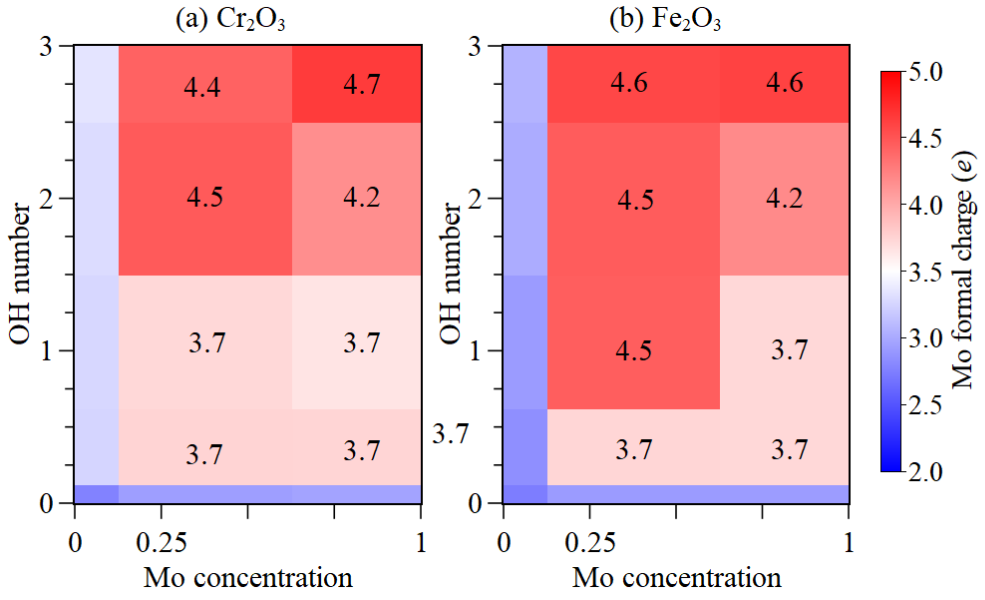

Figure 14. Formal charge of Mo (on Mo-substituted surfaces) and substituted Cr(Fe) atom (on Mo-free surfaces) on (0001)-oriented single-M-terminated (a) Cr_2O_3 and (b) Fe_2O_3 surfaces. The charge values are labelled for hydroxylated Mo-substituted surfaces. The substituted sites are "M2dn" and "M1dn" on anhydrous and hydrous surfaces, respectively. OH coverage and

Mo concentration are expressed in number per unit cell.

4. Conclusion

In this work we investigated the stability and the effect of substitutional Mo on hydroxylated (0001)-oriented Cr_2O_3 and Fe_2O_3 surfaces. The results allow us to draw the following conclusions:

- In dry air at room temperature, O-terminated (-Cr_2-O_3) and single-Fe-terminated (-O_3-Fe) surfaces are more favoured for Cr_2O_3 and Fe_2O_3, respectively, whereas in aqueous conditions, double-M-terminated surfaces with a high degree of hydroxylation (-O_3-Cr_2-$(OH)_3$ for Cr_2O_3 and -O_3-Fe_2-$(OH)_{2\sim3}$ for Fe_2O_3) are the most stable compared to other OH coverages and terminations.

- The presence of Mo in substitutional position favours the bare O-terminated surfaces in extremely oxidant conditions for both Cr_2O_3 and Fe_2O_3. In less oxidant aqueous conditions, the fully hydroxylated double-M-terminated surface (-O_3-Mo-Cr-$(OH)_3$) remains as the only stable hydrous surface for Cr_2O_3. For Fe_2O_3, a single-M-terminated hydroxylated surface (-O_3-Mo-$(OH)_2$) is also stable, as well as the double-M-terminated surfaces with a high degree of hydroxylation (-O_3-Mo-Fe-$(OH)_{2\sim3}$).

- The favoured location of substitutional Mo is in the subsurface planes on anhydrous surfaces, whereas OH surface loading “moves” the favoured location outwards in the cation surface plane. For fully hydroxylated surfaces, the DFT calculations show that Mo sits just under the hydroxyl groups, in agreement with the experimental studies which concluded to the location of Mo at the hydroxide/oxide interface of bilayered passive films.

- The present work confirms for hydroxylated surfaces the conclusion previously obtained on anhydrous surfaces, that substitution by Mo is exothermic and Mo preferentially substitutes on the surface of Fe- rather than on Cr-rich zones of the inner barrier layer of passive films.

- The formal charges of Mo on double-M-terminated surfaces are always near 3 *e*, regardless of the OH coverage, as well as on anhydrous single-M-terminated surfaces. In contrast, for OH-covered single-M-terminated surfaces, the charge localized on Mo increases to a higher level, reaching about 4.7 *e* on fully hydroxylated surfaces. This is consistent with the XPS experimental observations on passive films, in which Mo is at +4 or an intermediate state between +4 and +6 on hydrous oxide surfaces.

CRediT authorship contribution statement

Xian Huang: Conceptualization, Methodology, Formal analysis, Investigation, Writing – original draft, Writing – review & editing, Visualization.

Dominique Costa: Conceptualization, Methodology, Validation, Resources, Writing – review & editing, Supervision.

Boubakar Diawara: Conceptualization, Methodology, Software, Validation, Resources, Writing – review & editing, Supervision.

Vincent Maurice: Conceptualization, Methodology, Writing – review & editing, Supervision.

Philippe Marcus: Conceptualization, Methodology, Writing – review & editing, Supervision, Project administration, Funding acquisition.

Declaration of Competing Interest

The authors declare that they have no known competing financial interests or personal relationships that could have appeared to influence the work reported in this paper.

Data Availability

Data will be made available on request.

Acknowledgement

This work was supported by the European Research Council (ERC) under the European Union's Horizon 2020 research and innovation program (ERC Advanced Grant agreement No. 741123).

The authors acknowledge GENCI for high performance calculations in the national CEA centre under the agreement A0040802217 and the HPC resources of MesoPSL financed by the Region Ile de France and the project Equip@Meso (reference ANR-10-EQPX-29-01) of the programme Investissements d'Avenir supervised by the Agence Nationale pour la Recherche.

Appendix A: Atomic chemical potential

The hydroxylation of surfaces can occur in different environments. To determine the chemical

potentials μ_{O} and μ_{H} used in Equations (1) and (2), we consider here three possible references for the adsorbed O and H atoms on surfaces:

1) For hydroxylation of anhydrous surfaces in gaseous environments, O and H on hydrous surfaces may come from O_2 and H_2O gases, respectively. The considered reaction for surface hydroxylation is

$$n\mathrm{Cr_2O_3(bulk)} + \frac{1}{2}\left(3m + \frac{k}{2}\right)\mathrm{O_2(g)} + \frac{k}{2}\mathrm{H_2O(g)} \rightarrow \mathrm{Cr_{2n}O_{3(n+m)}} \cdot k\mathrm{OH(slab)} \quad (4)$$

Using ideal gas assumption, we have

$$\mu_{\mathrm{O}} = \frac{1}{2}G_{\mathrm{O_2(g)}} + \frac{1}{2}k_{\mathrm{B}}T\ln\left(\frac{P_{\mathrm{O_2}}}{P^0}\right) \quad (5)$$

$$\mu_{\mathrm{H}} = \frac{1}{2}G_{\mathrm{H_2O(g)}} - \frac{1}{4}G_{\mathrm{O_2(g)}} + \frac{1}{2}k_{\mathrm{B}}T\ln\left(\frac{P_{\mathrm{H_2O}}}{P^0}\right) - \frac{1}{4}k_{\mathrm{B}}T\ln\left(\frac{P_{\mathrm{O_2}}}{P^0}\right) \quad (6)$$

where G is the Gibbs free energy, k_{B} the Boltzmann constant, T the temperature, P^0 the standard pressure, and P the partial pressure. The saturated partial pressure of H_2O can be deduced from the free energy of water evaporation $\Delta G^0_{\mathrm{evap,H_2O}}$ obtained from the NIST database [41].

2) When anhydrous surfaces are hydroxylated in solution by water and dissolved oxygen gas, one has

$$n\mathrm{Cr_2O_3(bulk)} + \frac{1}{2}\left(3m + \frac{k}{2}\right)\mathrm{O_2(aq)} + \frac{k}{2}\mathrm{H_2O(l)} \rightarrow \mathrm{Cr_{2n}O_{3(n+m)}} \cdot k\mathrm{OH(slab)}. \quad (7)$$

The free energy of oxygen dissolved in water, $\Delta G_{\mathrm{sol,O_2}}$, can be deduced from the Henry's law [41] and used to calculate the chemical potential of oxygen. The free energy of liquid H_2O can be deduced from that of gaseous H_2O and the free energy of water evaporation $\Delta G^0_{\mathrm{evap,H_2O}}$. We have

$$\mu_{\mathrm{O}} = \frac{1}{2}G_{\mathrm{O_2(g)}} + \frac{1}{2}\Delta G_{\mathrm{sol,O_2}} + \frac{1}{2}k_{\mathrm{B}}T\ln\left(\frac{c_{\mathrm{O_2}}}{c^0}\right) \quad (8)$$

$$\mu_{\mathrm{H}} = \frac{1}{2}G_{\mathrm{H_2O(g)}} - \frac{1}{2}\Delta G_{\mathrm{evap,H_2O}} - \frac{1}{4}G_{\mathrm{O_2(g)}} - \frac{1}{4}\Delta G_{\mathrm{sol,O_2}} - \frac{1}{4}k_{\mathrm{B}}T\ln\left(\frac{c_{\mathrm{O_2}}}{c^0}\right) \quad (9)$$

where $c_{\mathrm{O_2}}$ and c^0 are the concentrations of dissolved oxygen in water and the standard concentration, respectively. The lower limit for O potential can be imposed by considering the reduction of chromium oxide to chromium metal in extremely oxygen-deficient environments.

3) If it is considered that the oxygen used for hydroxylation comes from water, as for an electrochemical passivation process in acid solution which produces hydrogen at the cathode, then the corresponding anodic and cathodic reactions are

$$n\mathrm{Cr_2O_3(bulk)} + (3m+k)\mathrm{H_2O(l)} \rightarrow \mathrm{Cr_{2n}O_{3(n+m)}} \cdot k\mathrm{OH(slab)} + (6m+k)\mathrm{H^+} + (6m+k)\mathrm{e^-} \quad (10)$$

$$\mathrm{H^+ + e^- \rightarrow \frac{1}{2}H_2(g).} \quad (11)$$

The approach of Nørskov *et al*. [42,43], called computational hydrogen electrode (CHE), can be applied in order to express the free energy of the anodic reaction using a standard hydrogen electrode (SHE) as reference electrode. The principle is detailed in Appendix B. The activities of water and hydrogen gas are considered as 1. With this approach, the chemical potentials can be written as

$$\mu_\mathrm{O} = G_{\mathrm{H_2O(g)}} - \Delta G_{\mathrm{evap,H_2O}} - G_{\mathrm{H_2(g)}} + 2\ln(10)\, k_\mathrm{B} T \mathrm{pH} + 2eU_\mathrm{SHE} \quad (12)$$

$$\mu_\mathrm{H} = \frac{1}{2} G_{\mathrm{H_2(g)}} - k_\mathrm{B} T \ln(10)\, \mathrm{pH} - eU_\mathrm{SHE} \quad (13)$$

where e is the elemental charge and U_SHE the applied potential referenced to SHE.

In the cases 2) and 3) with liquid water, the chemical potentials follow the relation

$$\mu_\mathrm{O} + 2\mu_\mathrm{H} = G_{\mathrm{H_2O(g)}} - \Delta G_{\mathrm{evap,H_2O}}. \quad (14)$$

In this study, the vibrational entropy and zero-point energy contributions to the free energy of reaction (i.e., surface formation and Mo substitution) were omitted, so the Gibbs free energies *G* were approximated by the DFT energies *E* for slabs, bulk and accordingly gases in the above equations of chemical potentials.

Appendix B: Application of Nørskov approach

Here we consider the anode surface S reacting with water to adsorb hydroxyl group and resulting in hydrogen gas production at the cathode in an electrochemical process, the total and half reactions are

$$\text{Total: } \mathrm{S + H_2O(l) \rightarrow S \cdot OH + \frac{1}{2}H_2(g)} \quad (15)$$

$$\text{Anode: } \mathrm{S} + \mathrm{H_2O(l)} \rightarrow \mathrm{S \cdot OH} + \mathrm{H^+(aq)} + \mathrm{e^-} \tag{16}$$

$$\text{Cathode: } \mathrm{H^+(aq)} + \mathrm{e^-} \rightarrow \tfrac{1}{2}\mathrm{H_2(g)}. \tag{17}$$

If the activities of water (solvent) and (pure) hydrogen gas are 1, the free energies of reactions can be written as

$$G_{\mathrm{tot}} = G_{\mathrm{S{\cdot}OH}} - G_{\mathrm{S}} + \frac{1}{2}G_{\mathrm{H_2(g)}} - G_{\mathrm{H_2O(l)}} \tag{18}$$

$$G_{\mathrm{a}} = G_{\mathrm{S{\cdot}OH}} - G_{\mathrm{S}} + G_{\mathrm{H^+(aq),pH=0}} - \ln(10)\, k_{\mathrm{B}} T \mathrm{pH} + G_{\mathrm{e^-},U=0} - eU - G_{\mathrm{H_2O(l)}} \tag{19}$$

$$G_{\mathrm{c}} = \frac{1}{2}G_{\mathrm{H_2(g)}} - G_{\mathrm{H^+(aq),pH=0}} + \ln(10)\, k_{\mathrm{B}} T \mathrm{pH} - G_{\mathrm{e^-},U=0} + eU \tag{20}$$

where U is the applied potential in V.

Using a standard hydrogen electrode for cathode (pH = 0), the free energy of cathode reaction (i.e., the hydrogen evolution reaction) should be 0 at zero applied potential:

$$\frac{1}{2}G_{\mathrm{H_2(g)}} - G_{\mathrm{H^+(aq),pH=0}} - G_{\mathrm{e^-},U_{\mathrm{SHE}}=0} = 0. \tag{21}$$

The free energy of liquid H_2O can be deduced from that of gaseous H_2O and the free energy of water evaporation $\Delta G^0_{\mathrm{evap,H_2O}}$. For anodic and cathodic reactions, we have

$$G_{\mathrm{a,SHE}} = G_{\mathrm{S{\cdot}OH}} - G_{\mathrm{S}} - G_{\mathrm{H_2O(g)}} + \Delta G_{\mathrm{evap,H_2O}} + \frac{1}{2}G_{\mathrm{H_2(g)}} - \ln(10)\, k_{\mathrm{B}} T \mathrm{pH} - eU_{\mathrm{SHE}} \tag{22}$$

$$G_{\mathrm{c,SHE}} = \ln(10)\, k_{\mathrm{B}} T \mathrm{pH} + eU_{\mathrm{SHE}}. \tag{23}$$

From the above equations we can extract the chemical potentials of OH and H, and then of O.

References

[1] B. Lynch, Z. Wang, L. Ma, E.-M. Paschalidou, F. Wiame, V. Maurice, P. Marcus, Passivation-induced Cr and Mo enrichments of 316L stainless steel surfaces and effects of controlled pre-oxidation, J. Electrochem. Soc. 167 (2020) 141509. https://doi.org/10.1149/1945-7111/abc727.

[2] Z. Wang, C. Carrière, A. Seyeux, S. Zanna, D. Mercier, P. Marcus, XPS and ToF-SIMS

investigation of native oxides and passive films formed on nickel alloys containing chromium and molybdenum, J. Electrochem. Soc. 168 (2021) 041503. https://doi.org/10.1149/1945-7111/abf308.

[3] X. Wang, D. Mercier, Y. Danard, T. Rieger, L. Perrière, M. Laurent-Brocq, I. Guillot, V. Maurice, P. Marcus, Enhanced passivity of Cr-Fe-Co-Ni-Mo multi-component single-phase face-centred cubic alloys: design, production and corrosion behaviour, Corros. Sci. 200 (2022) 110233. https://doi.org/10.1016/j.corsci.2022.110233.

[4] L. Ma, F. Wiame, V. Maurice, P. Marcus, Origin of nanoscale heterogeneity in the surface oxide film protecting stainless steel against corrosion, Npj Mater. Degrad. 3 (2019) 29. https://doi.org/10.1038/s41529-019-0091-4.

[5] L. Ma, B. Lynch, F. Wiame, V. Maurice, P. Marcus, Nanoscale early oxidation mechanisms of model FeCrNi austenitic stainless steel surfaces at room temperature, Corros. Sci. 190 (2021) 109653. https://doi.org/10.1016/j.corsci.2021.109653.

[6] X. Wang, D. Mercier, S. Zanna, A. Seyeux, L. Perriere, M. Laurent-Brocq, I. Guillot, V. Maurice, P. Marcus, Origin of enhanced passivity of Cr–Fe–Co–Ni–Mo multi-principal element alloy surfaces, Npj Mater. Degrad. 7 (2023) 13. https://doi.org/10.1038/s41529-023-00330-z.

[7] X. Wang, D. Mercier, S. Zanna, A. Seyeux, L. Perriere, M. Laurent-Brocq, I. Guillot, V. Maurice, P. Marcus, Effects of chloride ions on passive oxide films formed on Cr-Fe-Co-Ni(-Mo) multi-principal element alloy surfaces, J. Electrochem. Soc. 170 (2023) 041506. https://doi.org/10.1149/1945-7111/accb10.

[8] X. Huang, D. Costa, B. Diawara, V. Maurice, P. Marcus, Atomistic insights on enhanced passivity: DFT study of substitutional Mo on Cr2O3 and Fe2O3 surfaces, Corros. Sci. 224 (2023) 111543. https://doi.org/10.1016/j.corsci.2023.111543.

[9] V. Maurice, P. Marcus, Molybdenum effects on the stability of passive films unraveled at the nanometer and atomic scales, Npj Mater. Degrad. 8 (2024) 1–10. https://doi.org/10.1038/s41529-023-00418-6.

[10] V. Maurice, W.P. Yang, P. Marcus, XPS and STM investigation of the passive film formed on Cr(110) single-crystal surfaces, J. Electrochem. Soc. 141 (1994) 3016–3027. https://doi.org/10.1149/1.2059274.

[11] D. Zuili, V. Maurice, P. Marcus, In situ scanning tunneling microscopy study of the structure of the hydroxylated anodic oxide film formed on Cr(110) single-crystal surfaces, J. Phys. Chem. B 103 (1999) 7896–7905. https://doi.org/10.1021/jp9911088.

[12] V. Maurice, W.P. Yang, P. Marcus, XPS and STM study of passive films formed on Fe-22Cr(110) single-crystal surfaces, J. Electrochem. Soc. 143 (1996) 1182–1200. https://doi.org/10.1149/1.1836616.

[13] V. Maurice, W.P. Yang, P. Marcus, X-ray photoelectron spectroscopy and scanning tunneling microscopy study of passive films formed on (100) Fe-18Cr-13Ni single-crystal surfaces, J. Electrochem. Soc. 145 (1998) 909–920. https://doi.org/10.1149/1.1838366.

[14] V. Maurice, S. Cadot, P. Marcus, XPS, LEED and STM study of thin oxide films formed on Cr(110), Surf. Sci. 458 (2000) 195–215. https://doi.org/10.1016/S0039-6028(00)00439-8.

[15] H. Kuhlenbeck, C. Xu, B. Dillmann, M. Haßel, B. Adam, D. Ehrlich, S. Wohlrab, H.-J. Freund, U.A. Ditzinger, H. Neddermeyer, M. Neumann, M. Neuber, Adsorption and reaction on oxide surfaces: CO and CO_2 on Cr_2O_3(111), Berichte Bunsenges. Für Phys. Chem. 96 (1992) 15–27. https://doi.org/10.1002/bbpc.19920960104.

[16] Th. Gloege, H.L. Meyerheim, W. Moritz, D. Wolf, X-ray structure analysis of the Cr_2O_3(0001)-(1×1) surface: evidence for Cr interstitial, Surf. Sci. 441 (1999) L917–L923. https://doi.org/10.1016/S0039-6028(99)00870-5.

[17] M. Lübbe, W. Moritz, A LEED analysis of the clean surfaces of α-Fe_2O_3 (0001) and α-Cr_2O_3 (0001) bulk single crystals, J. Phys. Condens. Matter 21 (2009) 134010. https://doi.org/10.1088/0953-8984/21/13/134010.

[18] G. Ketteler, W. Weiss, W. Ranke, Surface structures of α-Fe_2O_3 (0001) phases determined by LEED crystallography, Surf. Rev. Lett. 08 (2001) 661–683. https://doi.org/10.1142/S0218625X01001610.

[19] X.-G. Wang, J.R. Smith, Surface phase diagram for Cr_2O_3 (0001) : *Ab initio* density functional study, Phys. Rev. B 68 (2003) 201402. https://doi.org/10.1103/PhysRevB.68.201402.

[20] A. Rohrbach, J. Hafner, G. Kresse, *Ab initio* study of the (0001) surfaces of hematite and chromia: Influence of strong electronic correlations, Phys. Rev. B 70 (2004) 125426. https://doi.org/10.1103/PhysRevB.70.125426.

[21] S.M.O. Souvi, M. Badawi, F. Virot, S. Cristol, L. Cantrel, J.-F. Paul, Influence of water, dihydrogen and dioxygen on the stability of the Cr_2O_3 surface: A first-principles investigation, Surf. Sci. 666 (2017) 44–52. https://doi.org/10.1016/j.susc.2017.08.005.

[22] S.M.O. Souvi, M. Badawi, J.-F. Paul, S. Cristol, L. Cantrel, A DFT study of the hematite surface state in the presence of H_2, H_2O and O_2, Surf. Sci. 610 (2013) 7–15.

https://doi.org/10.1016/j.susc.2012.12.012.

[23] X. Huang, S.K. Ramadugu, S.E. Mason, Surface-specific DFT + *U* approach applied to α-Fe_2O_3 (0001), J. Phys. Chem. C 120 (2016) 4919–4930. https://doi.org/10.1021/acs.jpcc.5b12144.

[24] M.A. Henderson, S.A. Chambers, HREELS, TPD and XPS study of the interaction of water with the α-Cr2O3(001) surface, Surf. Sci. 449 (2000) 135–150. https://doi.org/10.1016/S0039-6028(99)01246-7.

[25] M.H.M. Ahmed, X. Torrelles, J.P.W. Treacy, H. Hussain, C. Nicklin, P.L. Wincott, D.J. Vaughan, G. Thornton, R. Lindsay, Geometry of α-Cr_2O_3 (0001) as a Function of H2O Partial Pressure, J. Phys. Chem. C 119 (2015) 21426–21433. https://doi.org/10.1021/acs.jpcc.5b04607.

[26] V. Maurice, S. Cadot, P. Marcus, Hydroxylation of ultra-thin films of α-Cr2O3(0001) formed on Cr(110), Surf. Sci. 471 (2001) 43–58. https://doi.org/10.1016/S0039-6028(00)00880-3.

[27] R.L. Kurtz, V.E. Henrich, Surface electronic structure and chemisorption on corundum transition-metal oxides: α - Fe 2 O 3, Phys. Rev. B 36 (1987) 3413–3421. https://doi.org/10.1103/PhysRevB.36.3413.

[28] S. Yamamoto, T. Kendelewicz, J.T. Newberg, G. Ketteler, D.E. Starr, E.R. Mysak, K.J. Andersson, H. Ogasawara, H. Bluhm, M. Salmeron, G.E. Brown, A. Nilsson, Water Adsorption on α-Fe_2O_3 (0001) at near Ambient Conditions, J. Phys. Chem. C 114 (2010) 2256–2266. https://doi.org/10.1021/jp909876t.

[29] C.M. Eggleston, A.G. Stack, K.M. Rosso, S.R. Higgins, A.M. Bice, S.W. Boese, R.D. Pribyl, J.J. Nichols, The structure of hematite (α-Fe2O3) (001) surfaces in aqueous media: scanning tunneling microscopy and resonant tunneling calculations of coexisting O and Fe terminations, Geochim. Cosmochim. Acta 67 (2003) 985–1000. https://doi.org/10.1016/S0016-7037(02)01200-0.

[30] T.P. Trainor, A.M. Chaka, P.J. Eng, M. Newville, G.A. Waychunas, J.G. Catalano, G.E. Brown, Structure and reactivity of the hydrated hematite (0001) surface, Surf. Sci. 573 (2004) 204–224. https://doi.org/10.1016/j.susc.2004.09.040.

[31] T. Bredow, Embedded cluster study of water adsorption at Cr2O3(0001), Surf. Sci. 401 (1998) 82–95. https://doi.org/10.1016/S0039-6028(97)00913-8.

[32] D. Costa, K. Sharkas, M.M. Islam, P. Marcus, Ab initio study of the chemical states of water on Cr2O3(0001): From the isolated molecule to saturation coverage, Surf. Sci. 603

(2009) 2484–2493. https://doi.org/10.1016/j.susc.2009.05.037.

[33] D. Costa, P. Marcus, Electronic core levels of hydroxyls at the surface of chromia related to their XPS O 1s signature: A DFT+U study, Surf. Sci. 604 (2010) 932–938. https://doi.org/10.1016/j.susc.2010.02.023.

[34] S. Yin, X. Ma, D.E. Ellis, Initial stages of H2O adsorption and hydroxylation of Fe-terminated α-Fe2O3(0001) surface, Surf. Sci. 601 (2007) 2426–2437. https://doi.org/10.1016/j.susc.2007.04.059.

[35] Q. Pang, H. DorMohammadi, O.B. Isgor, L. Árnadóttir, Density functional theory study on the effect of OH and Cl adsorption on the surface structure of α-Fe2O3, Comput. Theor. Chem. 1100 (2017) 91–101. https://doi.org/10.1016/j.comptc.2016.12.009.

[36] R.B. Wang, A. Hellman, Surface terminations of hematite (α-Fe_2O_3) exposed to oxygen, hydrogen, or water: dependence on the density functional theory methodology, J. Phys. Condens. Matter 30 (2018) 275002. https://doi.org/10.1088/1361-648X/aac743.

[37] S. Maheshwari, Y. Li, M.J. Janik, The Fe_2O_3 (0001) Surface Under Electroreduction Conditions: A DFT Study of L-Cysteine Adsorption, J. Electrochem. Soc. 169 (2022) 064513. https://doi.org/10.1149/1945-7111/ac7826.

[38] Z. Futera, N.J. English, Water Breakup at Fe_2O_3 – Hematite/Water Interfaces: Influence of External Electric Fields from Nonequilibrium *Ab Initio* Molecular Dynamics, J. Phys. Chem. Lett. 12 (2021) 6818–6826. https://doi.org/10.1021/acs.jpclett.1c01479.

[39] M.-F. Ng, D.J. Blackwood, H. Jin, T.L. Tan, DFT study of oxygen reduction reaction on chromia and hematite: insights into corrosion inhibition, J. Phys. Chem. C 124 (2020) 13799–13808. https://doi.org/10.1021/acs.jpcc.0c03559.

[40] J. Neugebauer, M. Scheffler, Adsorbate-substrate and adsorbate-adsorbate interactions of Na and K adlayers on Al(111), Phys. Rev. B 46 (1992) 16067–16080. https://doi.org/10.1103/PhysRevB.46.16067.

[41] P.J. Linstrom, W.G. Mallard, eds., NIST Chemistry WebBook, NIST Standard Reference Database Number 69, National Institute of Standards and Technology, Gaithersburg, MD, 2022. https://doi.org/10.18434/T4D303.

[42] J.K. Nørskov, J. Rossmeisl, A. Logadottir, L. Lindqvist, J.R. Kitchin, T. Bligaard, H. Jónsson, Origin of the Overpotential for Oxygen Reduction at a Fuel-Cell Cathode, J. Phys. Chem. B 108 (2004) 17886–17892. https://doi.org/10.1021/jp047349j.

[43] H.A. Hansen, J. Rossmeisl, J.K. Nørskov, Surface Pourbaix diagrams and oxygen reduction

activity of Pt, Ag and Ni(111) surfaces studied by DFT, Phys. Chem. Chem. Phys. 10 (2008) 3722. https://doi.org/10.1039/b803956a.

[44] W. Tang, E. Sanville, G. Henkelman, A grid-based Bader analysis algorithm without lattice bias, J. Phys. Condens. Matter 21 (2009) 084204. https://doi.org/10.1088/0953-8984/21/8/084204.

[45] B. Diawara, ModelView, (n.d.). http://modelview.fr/.

Supporting information

Figure S1 shows the structures of relaxed anhydrous Fe_2O_3 surfaces. They are similar to those of Cr_2O_3 but with different spin ordering.

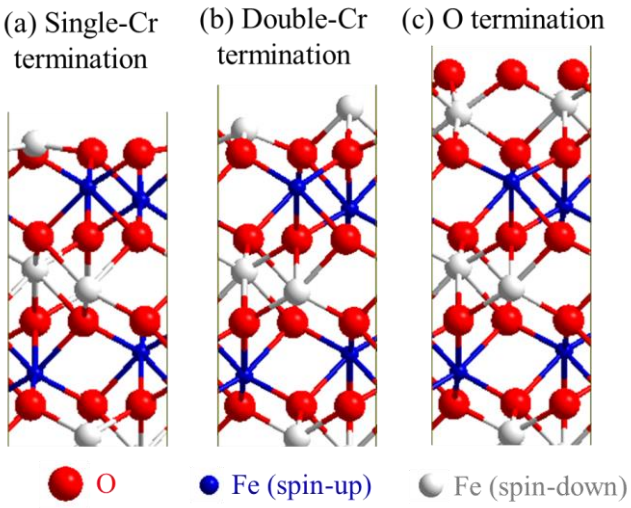

Figure S1. Side views of (0001)-oriented of anhydrous surfaces of Fe_2O_3 with different relaxed terminations.

Figure S2 shows the configuration of O-H bonds "tilted" and "normal" to the surface on hydrous single-Cr-terminated (M1; 0.25 OH; 0.25 OH/M) Cr_2O_3 surfaces. The structures with tilted bonds are always energetically more favoured than those with normal bonds, even with the presence of substitutional Mo.

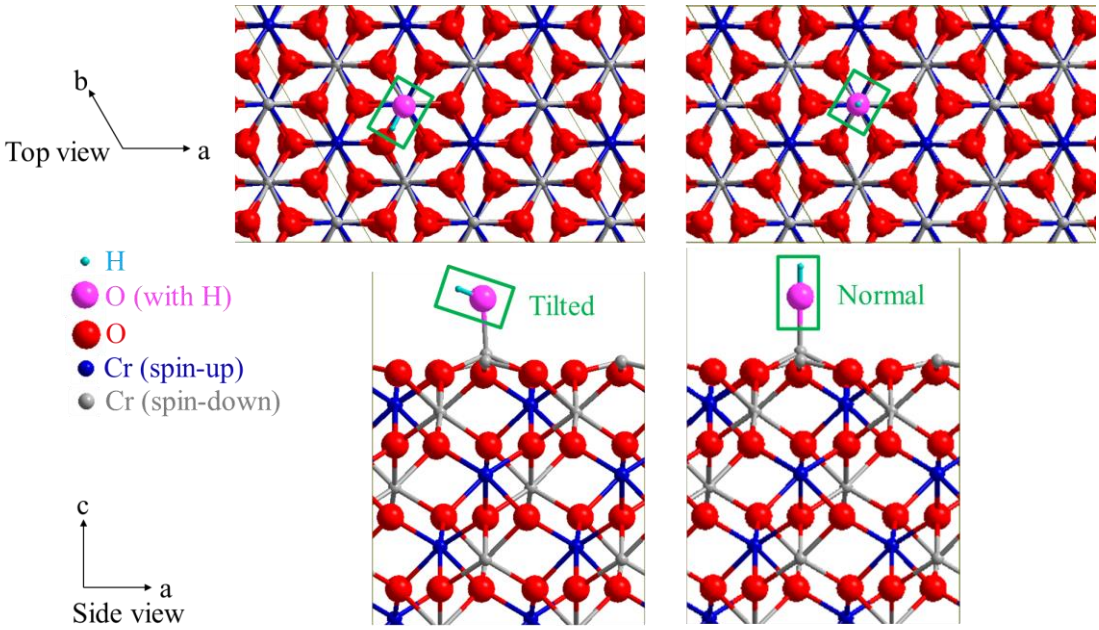

Figure S2. Configuration of "tilted" and "normal" O-H bonds on hydrous (0001)-oriented single-Cr-terminated (M1; 0.25 OH; 0.25 OH/M) Cr_2O_3 surfaces.

Figure S3 shows the free energies of anhydrous Fe_2O_3 surfaces. Only the single-Fe-terminated surface is favoured between the limits for O chemical potentials.

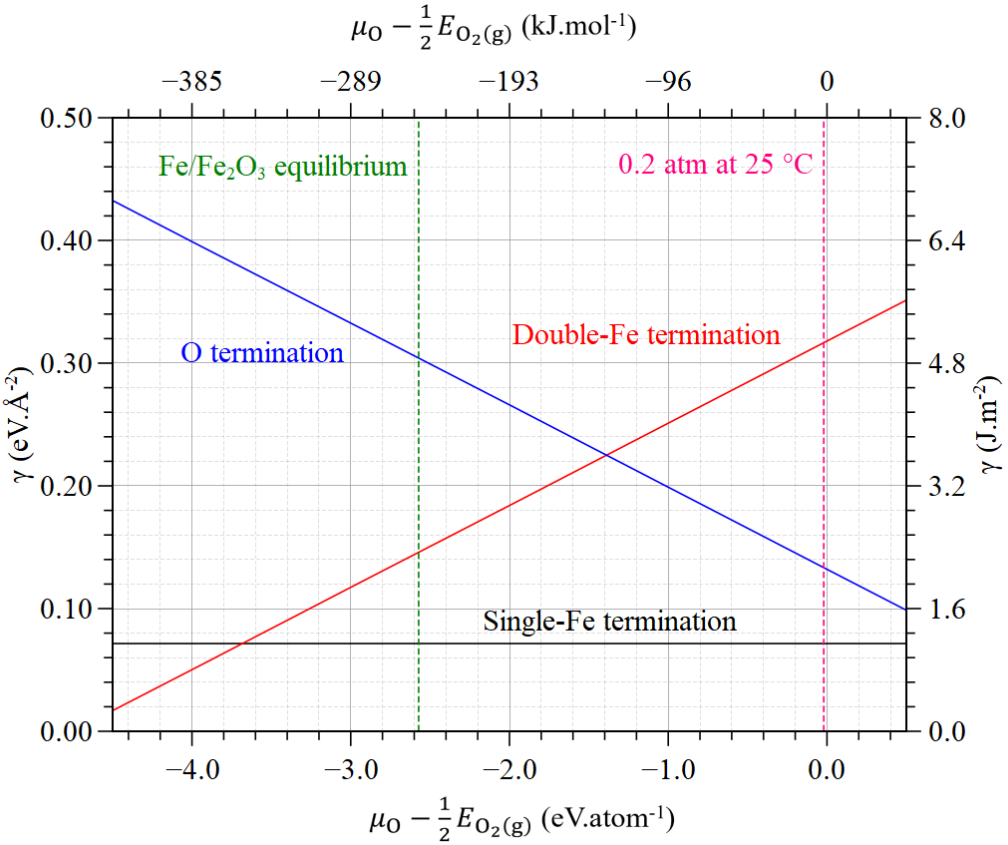

Figure S3. Surface free energies of different (0001)-oriented anhydrous Fe_2O_3 surface terminations.

Figure S4 shows the relative charges on Fe_2O_3 surfaces. The distributions are similar to those of Cr_2O_3.

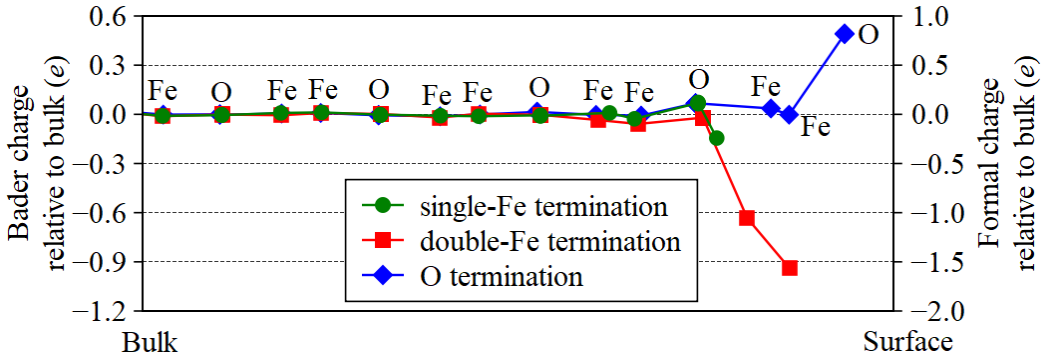

Figure S4. Bader and formal charges relative to bulk for anhydrous (0001)-oriented Fe_2O_3 surfaces with different terminations.

Figure S5 shows the structure of hydrous (0001)-oriented double-Fe-terminated (M2; 0.25 OH; 0.125 OH/M) Fe_2O_3 surfaces. One O atom on the surface (marked in light red) move into the terminating Fe plane, which is not observed on the Cr_2O_3 surface with the same OH coverage. The structures of the other hydrous Fe_2O_3 surfaces are similar to those of Cr_2O_3 surfaces.

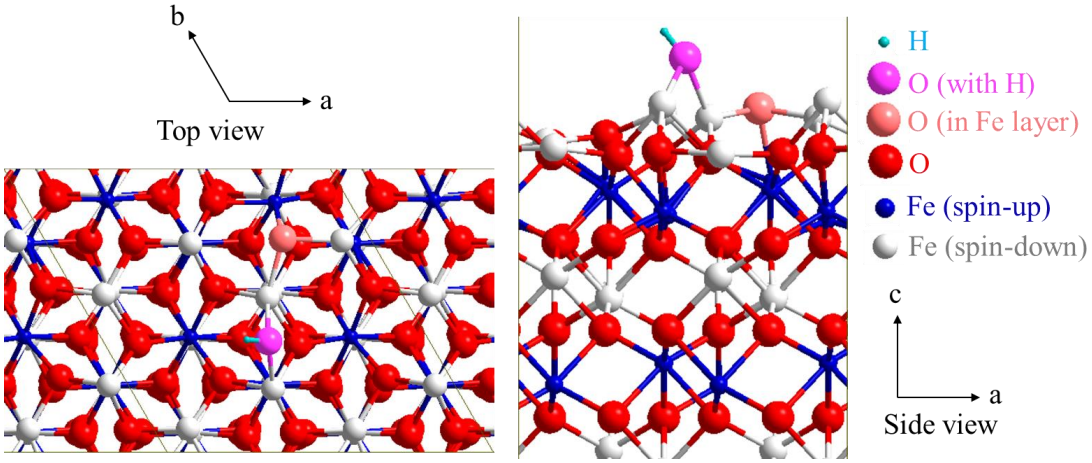

Figure S5. Top and side views of hydrous (0001)-oriented double-Fe-terminated (M2; 0.25 OH; 0.125 OH/M) Fe_2O_3 surfaces.

Figure S6 shows the free energies of anhydrous and hydrous Cr_2O_3 surfaces as function of applied potential in electrochemical process. The fully hydroxylated double-Cr-terminated surface (M2; 3 OH; 3 OH/M) is the most stable between the potential limits.

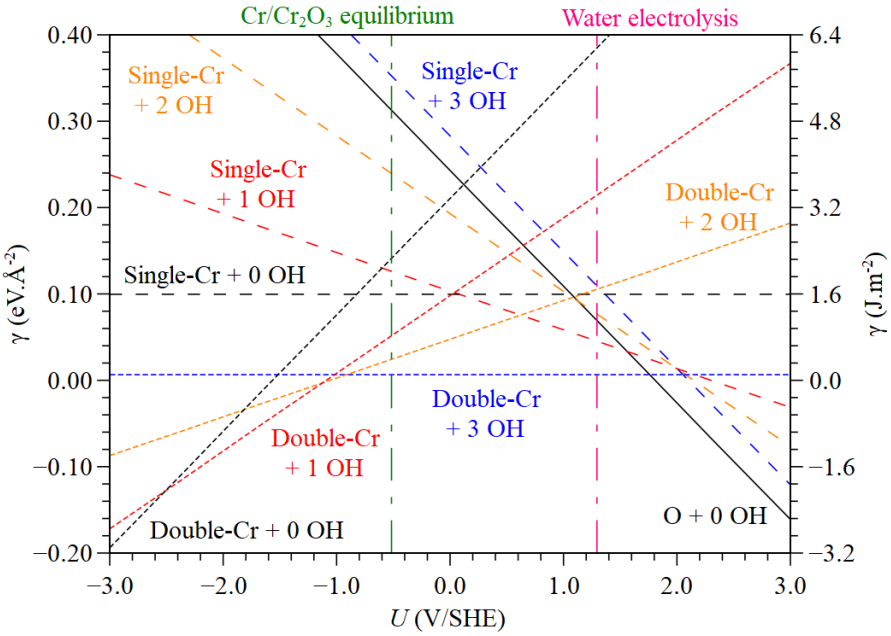

Figure S6. Surface free energies for (0001)-oriented Cr_2O_3 in electrolyte at pH = 0 and 25 °C. Termination and number of added hydroxyl groups are indicated.

Figure S7 shows the surface free energies in the case of electrochemical process. Between the limits of O chemical potential or applied potential, the stable surfaces can only be highly hydroxylated double-Fe-terminated surfaces (M2; 2 ~ 3 OH; 1 ~ 1.5 OH/M).

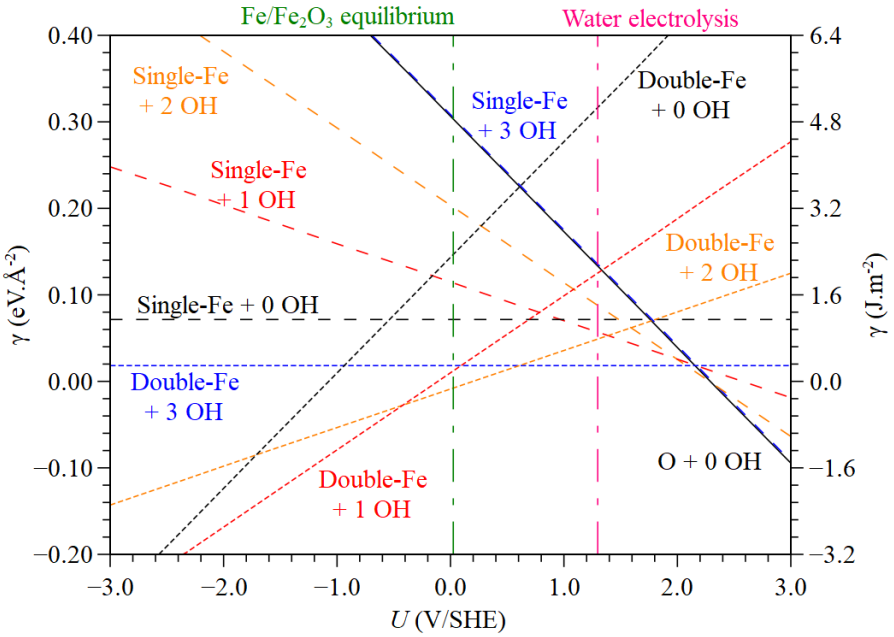

Figure S7. Surface free energies for (0001)-oriented Fe_2O_3 surfaces in electrolyte at pH = 0 and 25 °C.

Figure S8 shows the energy of substitution by Mo on Fe_2O_3 surface. The “M1dn” site is the

most stable, as on Cr_2O_3 hydrous surfaces.

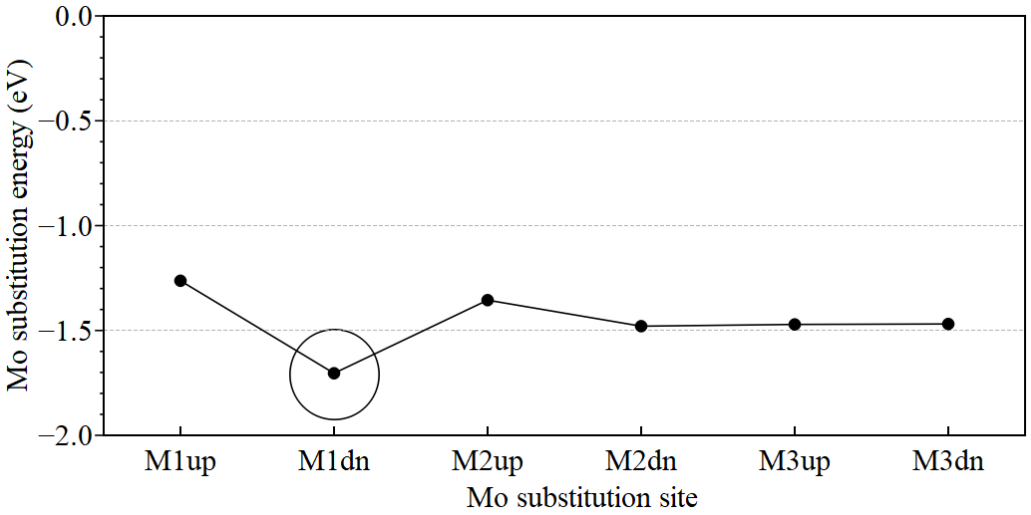

Figure S8. Energy of substitution by Mo on different cations sites for the fully hydroxylated, (0001)-oriented double-Fe-terminated Fe_2O_3 surface (M2; 3 OH; 1.5 OH/M) (substitution with high Mo concentration).

Table S1 shows the DFT energies of surfaces with different terminations and Mo loading. The DFT energies per atom of Cr, Fe and Mo are -6.81, -5.39 and -4.03 eV, respectively. The energies of substitution on different surfaces in Figure 13 are calculated using these values.

Table S1. DFT energies of Cr_2O_3 and Fe_2O_3 surfaces per 1×1 unit slab.

		Cr_2O_3			Fe_2O_3		
		0 Mo	0.25 Mo	1 Mo	0 Mo	0.25 Mo	1 Mo
Single-M	0 OH	-230.64	-230.14	-228.65	-203.32	-203.42	-203.68
	0.25 OH	-233.35	-232.97	-231.33	-205.83	-206.09	-205.69
	1 OH	-241.48	-241.11	-239.98	-213.27	-213.96	-214.38
	2 OH	-250.41	-250.78	-250.42	-222.20	-223.26	-224.84
	3 OH	-259.33	-260.00	-259.99	-230.77	-231.78	-234.41
Double-M	0 OH	-243.37	-243.53	-241.25	-213.07	-214.64	-213.51
	0.25 OH	-247.55	-247.01	-245.34	-218.00	-218.05	-218.00
	1 OH	-256.80	-256.25	-254.65	-226.99	-227.04	-227.12
	2 OH	-268.85	-268.30	-266.81	-238.34	-238.33	-238.25
	3 OH	-280.68	-280.50	-278.68	-248.65	-249.34	-249.00